

Single-antenna Low-power Spread Spectrum Adaptive Echo Cancellation System

by

Zhuo Li

B.Sc.E., Beijing University of Posts and Telecommunications
& Queen Mary College, University of London, 2009

A THESIS SUBMITTED IN PARTIAL FULFILLMENT OF THE
REQUIREMENTS FOR THE DEGREE OF

Master of Science in Engineering

In the Graduate Academic Unit of Electrical and Computer Engineering

Supervisor: Brent R. Petersen, Ph.D., Electrical and Comp. Eng

Examining Board: Peter J. Kyberd, Ph.D., Electrical and Comp. Eng, Chair
Julian Meng, Ph.D., Electrical and Comp. Eng
Richard J. Tervo, Ph.D., Electrical and Comp. Eng
Wei Song, Ph.D., Faculty of Computer Science

**This thesis is accepted by the
Dean of Graduate Studies**

THE UNIVERSITY OF NEW BRUNSWICK

April, 2012

© Zhuo Li, 2012

To my parents and Vicki.

Abstract

Full-duplex wireless communication networks need to deal with echo signals in order to obtain good performance, which could be achieved by using an echo canceller. By using multiple transmitters and receivers to relay the desired signal, dynamic ranges are reduced. This improvement will allow echo cancellation be effective. In this thesis, a single antenna, low-power full-duplex communication network architecture that is enabled to be used in a co-operative communication network is proposed. In addition to co-operative communication and echo cancellation, spread spectrum is also used to obtain high robustness against noise and interference. This network architecture is expected to work in 5.775 GHz ISM band with a 150 MHz bandwidth, with the requirement that spreading sequences for the proposed system must have both good autocorrelation and cross correlation properties. In regards to the above requirement, Gold sequences exhibit the best performance comparing to Frank-Heimiller sequences and m sequences. This network architecture is originally designed for an urban residential network. However, it could be applied to different fields and combined with different technologies.

Acknowledgements

I would like to thank my supervisor Brent Petersen for his generous support and guidance throughout my research work. He had spent his precious personal time to help me with my thesis, my research work as well as my future career planning. He also helped me with my research skills and polish my english writing skills.

I would like to thank professor Richard Tervo for his advice on complex spreading sequence generation method as well as DSSS system simulation.

I would like to thank Dr. A. Brown for his guidance in the area of circulator and channel isolation, and Denise Burke, Karen Annett, and Shelley Cormier from the ECE office for their kindness and support.

My thanks also go out to the Yaosuo Xue at Siemens Corporate Research for his support and his professional advice.

Table of Contents

Dedication	ii
Abstract	iii
Acknowledgments	iv
Table of Contents	v
List of Tables	ix
List of Figures	x
Abbreviations	xii
1 Introduction	1
1.1 Background and Literature Review	2
1.2 Thesis Contribution	5
1.3 Thesis Structure	6
2 System Model Description, Requirement and Design	7
2.1 Overview	7
2.1.1 Node Architecture	8
2.1.2 System Communication Overview	9
2.2 Circulator Design Decisions	13

2.2.1	Conventional Circulator	13
2.2.2	Circulator Requirements	16
2.2.3	Innovative Circulator Design	17
2.3	EC Design Decisions	19
2.3.1	Conventional Linear EC	19
2.3.2	EC with an On-off Switch	20
2.3.3	Adaptive Algorithm	22
2.4	Spread Spectrum Design Decision	23
2.4.1	The Spread Spectrum System	23
2.4.2	Architecture of DSSS	24
2.4.3	PN Sequence Generation	26
2.5	Equalizer Design Decision	28
3	System Analysis	30
3.1	System Outage Probability	30
3.1.1	Probability of Error for BPSK	31
3.1.2	Probability of Error for DSSS	31
3.1.3	Probability of Error for the Proposed System	32
3.2	Link Budget	33
3.2.1	Link Budget Analysis Criteria	33
3.2.2	Specific Link Budget Analysis	38
3.3	Design Trade-offs	40
3.3.1	Spreading Factor Exponent k and Power $P_{t,dBm}$	43
3.3.2	Spreading Factor Exponent k and Channel Gain A	44
3.4	Spreading Code	44
3.4.1	Performance of m Sequences/Gold Sequences	45
3.4.2	Performance of FH Sequences	47
3.4.3	Performance of Pseudo-randomly Generated Sequences	48

4	Simulation and Results	50
4.1	Simulation Setup	50
4.1.1	Channel Model	51
4.2	Simulation Results	54
4.2.1	Results for System Testing	54
4.2.2	Results for Trade-offs	59
4.2.3	Results for Different Spreading Codes	62
5	Summary and Future Work	67
5.1	Summary of Work Completed	67
5.2	Future Work	68
	Bibliography	70
	Appendices	75
A	Derivation of Equations	75
A.1	Derivation of Trade-off Equations	76
A.2	Derivation of Excess Bandwidth	76
B	MATLAB[®] Simulation Source Code	79
B.1	Simulation Parameter Set Up	79
B.2	Wireless Channel Impulse Response Generation	81
B.3	Simulation Driver	83
B.4	Simulation Parameter Set Up	90
B.5	Function of Root of Unity	94
B.6	Function of Convolution	95
B.7	Function of Decimated PN Sequences	96
C	Table of Irreducible Polynomials	97

Vita

List of Tables

3.1	Trade-off between k and $P_{t,dBm}$	43
3.2	Trade-off between k and A_{dB}	44
3.3	Comparison of Different Spreading Codes	48
A.1	Explanation of Equations	77
C.1	Meanings of Letters for Primitive Polynomials	97

List of Figures

1.1	Wireless Co-operative Communication Network	3
2.1	Simplified System Model	10
2.2	Signal Flow Diagram for a Single Node	14
2.3	Conventional Circulator Structure	15
2.4	New Circulator Structure [1]	18
2.5	EC Structure	20
2.6	EC with an On-off Detector	22
2.7	Model of Direct-Sequence Spread Spectrum	25
2.8	PN Sequence Generator	26
2.9	Gold Sequence Generator	27
2.10	The RAKE Receiver	29
3.1	Measured NLOS path gain as a function of Distance for the 5 GHz Band [2].	35
3.2	Measured LOS path gain as a function of Distance for the 5 GHz Band [2].	36
3.3	Flow Chart for Link Budget Analysis	40
4.1	Equalizer Coefficients	55
4.2	Equalizer Learning Curve	56
4.3	EC Coefficients	57
4.4	EC Learning Curve	58

4.5	Trade-off between k and $P_{t,dBm}$	60
4.6	Trade-off between k and A	61
4.7	Equalization Learning Curve for Gold Sequences	63
4.8	EC Learning Curve of Gold Sequences	64
4.9	EC Learning Curve of FH Sequences	65
4.10	Equalization Learning Curve of FH Sequences	66

List of Symbols, Nomenclature or Abbreviations

ATDD	Analog Time Division Duplex
AF	Amplify and Forward
AWGN	Additive White Gaussian Noise
BER	Bit Error Rate
BPSK	Binary Phase Shift Keying
CDMA	Code Division Multiple Access
dB	DeciBels
dBm	DeciBels relative to one milliwatt
DF	Decode and Forward
DSSS	Direct-Sequence Spread Spectrum
EC	Echo Cancellor
ERLE	Echo Return Loss Enhancement
FDD	Frequency-Division Duplex
FH	Frank-Heimiller
FHSS	Frequency Hopping Spread Spetrum
FT	Fourier Transform
GHz	Giga Hertz
HF	High Frequency

IEEE	Institute of Electrical and Electronics Engineers
ISI	Intersymbol Interference
ISM	Industrial, Scientific, and Medical
LOS	Line of Sight
LMS	Least Mean Square
LTE	Long Term Evolution
MHz	Mega Hertz
MIMO	Multiple-Input-Multiple-Output
MMSE	Minimum Mean-Squared-Error
MPSK	M-Phase Shift Keying
NLMS	Normalized LMS
NLOS	Non Line of Sight
ns	Nano Second
OLOS	Obstructed Line of Sight
PDP	Power Delay Profile
PG	Processing Gain
PN	Pseudorandom Noise
QAM	Quadrature Amplitude Modulation
QPSK	Quadrature Phase Shift Keying
RAKE	RAKE Receiver
RFID	Radio Frequency Identification
RF	Radio Frequency
RLS	Recursive Least Square
rms	Root Mean Square
SDMA	Spatial Division Multiplexing Access
SNR	Signal-to-Noise Ratio
TDD	Time-Division Duplex

UWB Ultra Wide Band

Chapter 1

Introduction

The idea of conventional full-duplex communication came originally from the need to provide efficient services to users of an application such as a wired telephony system [3]. In such a system, users can talk and listen simultaneously through two different wires. While in the wireless communication, full-duplex often refers to a FDD (Frequency-Division Duplex) [4] or a TDD (Time-Division Duplex) [4] system. Both of the technologies require division of either the frequency band or the time frame. In this thesis, full-duplex communication refers to both the forward link and the reverse link occupying the same frequency band and yet transmitting simultaneously. It has the advantage of wider bandwidth for both forward and reverse link and offers a more flexible means of communication. In modern telephone systems, wired full-duplex systems have been a dominant research topic and many significant results have been uncovered. With optical fibre and Ethernet being widely deployed, full-duplex technology has become mature.

As for wireless communication, full-duplex communication became more eminent. The difficulties mainly come from echo cancellation, which has been solved in wired communication environments. However, in wireless communication, echo cancellers (ECs) are often unable to handle the large dynamic ranges due to the low

channel attenuation. Also, intricate building structures could cause severe attenuation and heavy traffic leads to wireless channels with time-varying properties. Moreover, due to construction material in urban areas being mostly concrete and metal and due to the high building density in these areas, enormous signal reflections and scatterers causes multipath propagation. Similar characteristics could be expected for the indoor transmission environment which has smaller transmission distances but stronger multipath propagation. With such hostile transmission environments for full-duplex communication, critical solutions are needed. Nowadays with the dawning of cooperative wireless communication and multiple-input-multiple-output (MIMO) techniques, new technologies have been developed that can be embraced as new elements of full-duplex transmission. This includes beamforming, space-time coding/processing, SDMA (Spatial Division Multiplexing Access) and network MIMO. A review of full-duplex communication concepts developed in recent years leads to the requirement for a new communication network architecture and associated protocols enabling full-duplex access.

1.1 Background and Literature Review

This thesis proposes a full-duplex low-cost high-reliability co-operative communication system that could be applied to different fields and combined with different technologies. There are a plethora of radio system communication standards and each has been developed with specific applications under consideration, of which Long-term Evolution (LTE) Advanced is one of the most competitive systems. However, a full-duplex communication network requires communication systems with a high reliability as well as a high transmission rate in order to satisfy the requirements of next generation wireless communications. It is not a burden to propose another radio standard because many radio systems have multi-function capability, as dictated

by the controlling software, and the proposed communication system solves resource allocation issues in a co-operative communication [5].

The low-cost will be obtained through nodes having individual globally unique identification codes and using echo cancellation and full-duplex communication over a shared frequency band. Based on manufacturing, with globally unique code words assigned to each one of the nodes, they could communicate with each other simultaneously without interference. The co-operative communication will be achieved by implementing wireless relays between nodes in order to enhance coverage as well as increase the capacity of the network, as shown in Figure 1.1.

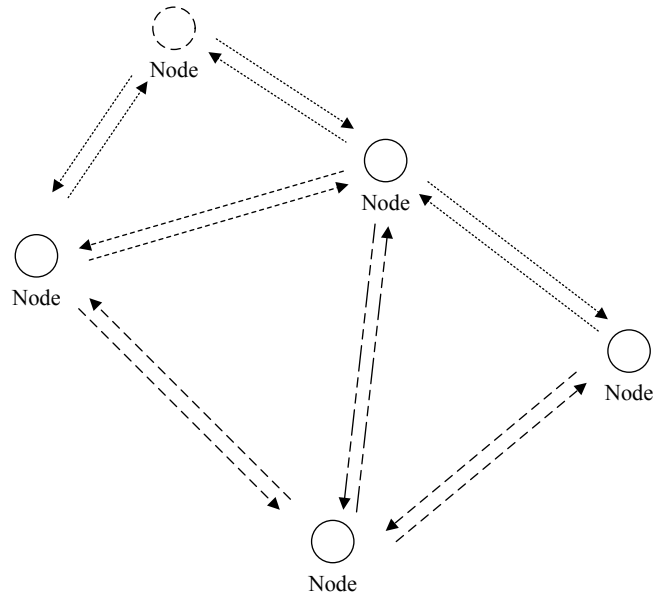


Figure 1.1: Wireless Co-operative Communication Network

Unlike the conventional one-hop cells, relays are low cost, transmit at a power level and are easy to deploy. Two of the most common relays can be classified into Amplify and Forward (AF) [6] and Decode and Forward (DF) [7]. The AF amplifies the received signal by a linear scale before resending it while the DF decodes the signal and then recodes it before the next step. Both relays can be operating in half-duplex and full-duplex modes. Lo and Guan have compared the performance of AF and

DF in full-duplex [8]. Other work has concentrated on comparing performance between half-duplex and full-duplex communication as well as investigating capacity of wireless full-duplex systems [9, 10]. The full-duplex capability is achieved by echo cancellation which is required under certain conditions among the design constraints of bit error rate, bit rate, bandwidth, transmission distance, and expected radio signal fading. For a full-duplex communication system, one of the main challenges is to achieve both forward and reverse link transmission simultaneously without interference from each other. During the past two decades, research has mainly focused on half-duplex system development with a small portion which evaluated the possibility of full-duplex wireless communication systems. Acoustic full-duplex systems became one of the most interesting topics with some results such as the ATDD (Analog Time Division Duplex) system for speech in HF (High Frequency) [11] and virtual full-duplex systems via rapid on-off-division duplexing [12]. Recently, research related to full-duplex wireless systems has embraced a breakthrough. Pelissier et al. have proposed a full-duplex Ultra Wide Band (UWB) Radio Frequency Identification (RFID) transceiver for wireless non-volatile memory application [13] while Omer et al. have proposed a self-jammed system to allow full-duplex operation in the presence of non-linear microwave components [14]. Similar work can be found in the paper written by Choi et al. [5] and the paper written by Duarte and Sabharwal [15]. In the paper written by Choi et al. [5], full-duplex communication is achieved by applying antenna cancellation while in Duarte and Sabharwal's work, full-duplex communication is achieved by applying a combination of antenna separation, digital cancellation and analog cancellation [15]. Both approaches focus on the application of multiple antennas. Although multiple antennas will bring a positive contribution to combatting multipath interference and severe received power distortion, the placement as well as the direction of the antennas needs to be carefully considered and adjusted, which imposes limitations in practice. In this thesis, the proposed system applies a single

antenna in conjunction based on a circulator. It alleviates the need for frequency planning by using each frequency band in a full-duplex mode and within a band using spread spectrum to multiplex the nodes' signals, which is an alternative approach to achieve a full-duplex system with fewer constraints.

1.2 Thesis Contribution

The main contribution of this thesis is the analysis, design and simulation of a full-duplex communication in the indoor environment. All effort up to now has been dedicated to design and verification of the basic node architecture based on full-duplex communication. The work is at the physical layer where each manufactured node uses a radio interface which allows all nodes to mutually simultaneously self-configure, synchronize, and communicate.

In this thesis, a basic physical layer node architecture for full-duplex communication is designed and verified. It is designed as a transceiver that could be mass produced and deployed. It is expected to be working in the 5 GHz industrial, scientific, and medical (ISM) band with a 150 MHz bandwidth. The architecture could be implemented to adapt to different transmission environments by adjusting parameters of each component. For example, by lowering the bit rate, the transmission distance could be extended to hundreds of meters. Secondly, several system performance prediction equations for the proposed system, from which some of the trade-offs as well as the relationships between different factors of the system designs can be shown, have been derived in the thesis. One of the derivations is the equation that shows the capability of DSSS (Direct Sequence Spread Spectrum). Thirdly, the effect of spreading sequences to the proposed system is investigated in the thesis. From the comparison among Gold sequences [4], Frank-Heimiller (FH) sequences [16] and the pseudo-randomly generated complex sequences we have summarized the requirement

of the spreading sequences.

1.3 Thesis Structure

The remainder of this document is broken down into four chapters. [chapter 2](#) describes the system requirements analysis, high-level design decisions, and the subsequent architecture design process. [chapter 3](#) outlines the details of the system analysis, and [chapter 4](#) describes the software simulation results along with some analysis and discussions. [chapter 5](#) summarizes the work completed in the thesis and outlines potential future work for the project.

Chapter 2

System Model Description, Requirement and Design

2.1 Overview

The design of a low-cost full-duplex communication system, just like any other communication system design, should be based on a specific application, transmission environment and carrier frequency. Hence, it is crucial to first understand the requirements of the system. The proposed system is expected to be able to handle both the outdoor transmission environment with a strong Line-of-Sight (LOS) path, time-varying aspects, a strong channel attenuation due to large distances and the indoor transmission environment with a strong Non Line-of-Sight (NLOS) component, relatively constant aspects, a strong Inter-Symbol-Interference (ISI) due to complicated indoor structure. As mentioned previously, in this case, we are more concerned about the indoor transmission environment. In order to obtain a wider bandwidth and less interference from other electronic devices, the carrier frequency for the proposed system is set to be working with the 5 GHz ISM band with the central frequency at 5.775 GHz and a 150 MHz bandwidth. The 5 GHz band holds the

advantages of a wider bandwidth, less inter-device interference than in the 2.4 GHz (i.e. the microwave ovens) and is also a member of the ISM band group. However, regarding such a high frequency, the wavelength λ of the 5 GHz band is relatively small which leads to more interference from the multipath propagation within an indoor environment.

2.1.1 Node Architecture

The node architecture of the proposed system is shown in [Figure 2.1](#). We use $b_{1,n}$ to denote the discrete data symbol transmitted from Node 1 (N_1) with a sampling rate equals to the symbol rate, $s_{1,m}$ to denote the transmitted signal with Direct-Sequence Spread Spectrum (DSSS) and a sampling rate equals to the chip rate. The symbol $h_{11,m}$ denotes the echo channel response for N_1 , $h_{12,m}$, $h_{13,m}$ to $h_{1u,m}$ denote the channel response to Node (N_1) from Node (N_2) to Node (N_u), respectively. The symbols $\hat{b}_{2,n}$ to $\hat{b}_{u,n}$ denote the received symbol signals from N_2 to N_u , respectively. For the purpose of building a network, the node architecture is designed to have the ability of handling signals from multiple nodes. Each node is designed to contain multiple receivers with each of the receivers responsible for receiving signals from a designated node. Signals from different nodes will be picked up by a single antenna and distinguished by unique spreading sequences. These sequences will be pre-installed in each of the receiver. Hence, much like designing a static Ethernet, the proposed full-duplex co-operative network can be easily designed by carefully arranging the router list within each of the nodes. Similarly, we use $b_{2,n}$ to denote the signal transmitted from N_2 with a sampling rate equals to the symbol rate, $s_{2,m}$ to denote the transmitted signal with the spread spectrum system and a sampling rate equals to the chip rate. $h_{22,m}$ denotes the echo channel response for N_2 and $h_{12,m}$ denotes the channel response from N_2 to N_1 . The notation $\hat{b}_{1,n}$ to $\hat{b}_{u,n}$ (except $\hat{b}_{2,n}$) denotes the received signal from N_1 to N_u (excluding N_2), respectively.

The received signal $r_{1,m}$ is the summation of the echo signal as well as signals from all other nodes. Similarly, $r_{2,m}$ denotes the summation of the echo signal as well as signals from all other nodes. Both the transmitted signal and the received signal share the same antenna through a circulator. Also, we use RAKE to denote a RAKE receiver. The DSSS at the receiver end represents the despreading process of the spread spectrum signal. Each node contains multiple receivers for other nodes. The symbol D denotes the distance between nodes.

A detailed node architecture is shown in [Figure 2.2](#), where $b_1[n]$ is the same as $b_{1,n}$, $b_2[n]$ is the same as $b_{2,n}$, $\hat{b}_2[n]$ is the same as $\hat{b}_{2,n}$, C_1 is the circulator coefficient, $t_1[m]$ is the final output of the antenna of N_1 , $g_2[m]$ to $g_4[m]$ are the received attenuated signals from N_2 to N_4 , $c_1[m]$ to $c_4[m]$ are the spreading sequences, $r_1[m]$ is the received signal with the local echo signal, $y_{12}[m]$ is the received signal after echo cancellation process and $e_{c1}[m]$ and $e_{e12}[n]$ are the *error* of the EC and the equalizer, respectively. Notice that the subscripts of $e_{e12}[n]$ indicates that it is the *error* of the equalizer for the received signal from N_2 . $w_1[m]$ and $\hat{w}_{12}[m]$ are the coefficient vectors of the EC and the equalizer, respectively. Notice that the subscripts of $\hat{w}_{12}[m]$ indicates the it is the coefficient vector of the equalizer for the received signal from N_2 .

2.1.2 System Communication Overview

For N_1 , the transmitted symbol $b_{1,n}$ is designed to be sent through the DSSS spreader and becomes $s_{1,m}$, where $s_{1,m} = d_{1,m} * c_{1,m}$, $s_{2,m} = d_{2,m} * c_{2,m}, \dots, s_{u,m} = d_{u,m} * c_{u,m}$ for N_1 to N_u , $d_{u,m}$ denotes the up-sampled data signal and $*$ denotes the convolution operation. $c_{1,m}$ to $c_{u,m}$ are the spreading sequences for each node. $s_{1,m}$ to $s_{u,m}$ are then sent through the wireless channels and picked up by antennas of other nodes. Take N_1 as an example, the received signal for N_1 is shown in [Equation 2.1](#),

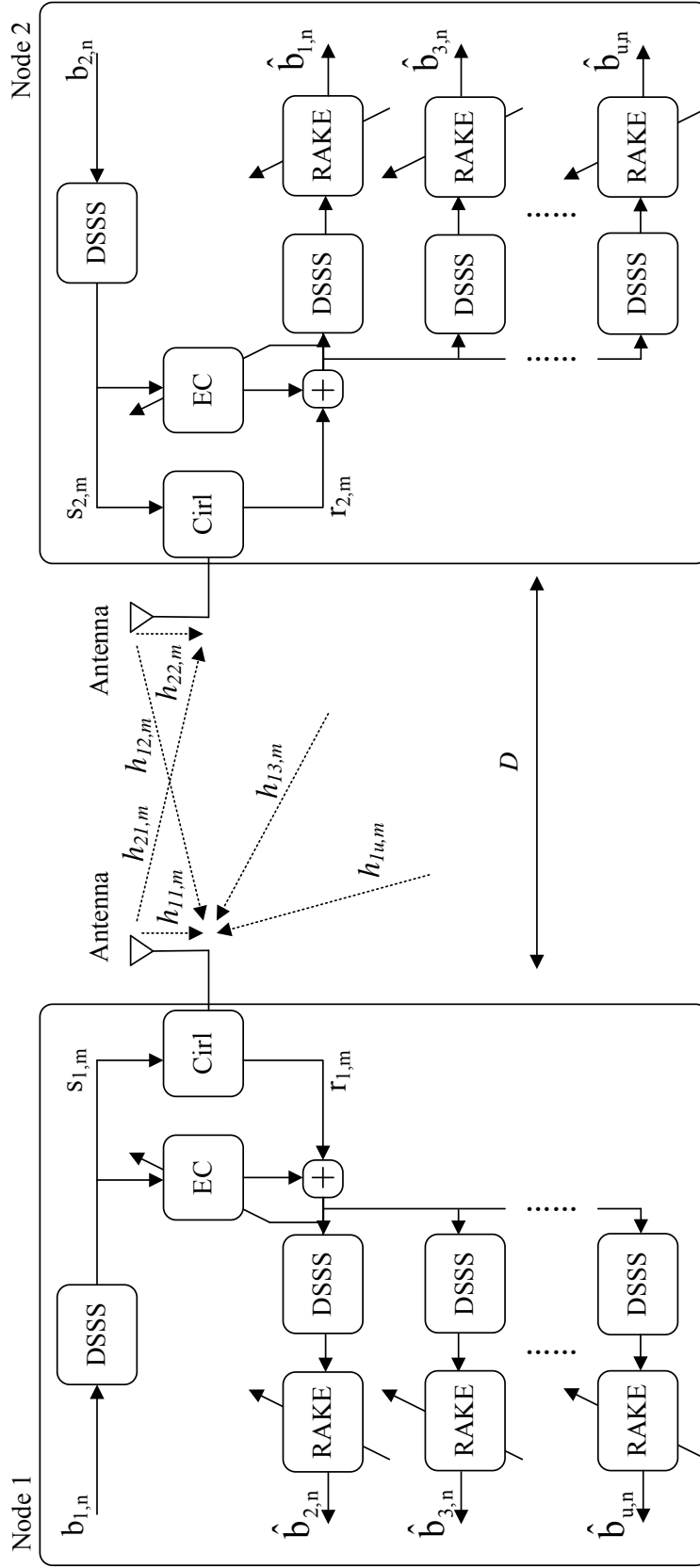


Figure 2.1: Simplified System Model

$$r_{1,m} = s_{1,m} * h_{11,m} + s_{2,m} * h_{12,m} + s_{3,m} * h_{13,m} + \dots + s_{u,m} * h_{1u,m} + \eta_{1,m}, \quad (2.1)$$

where $h_{11,m}$ indicates the echo channel response, $h_{12,m}$ to $h_{1u,m}$ indicate the wireless channel responses between N_1 and N_2 to N_u , $\eta_{1,m}$ indicates the additive white Gaussian noise (AWGN) for N_1 . Similarly, the received signals for N_2 to N_u are shown in [Equation 2.2](#),

$$\begin{aligned} r_{2,m} &= s_{2,m} * h_{22,m} + s_{1,m} * h_{21,m} + s_{3,m} * h_{23,m} + \dots + s_{u,m} * h_{2u,m} + \eta_{2,m} \\ r_{u,m} &= s_{u,m} * h_{uu,m} + s_{1,m} * h_{u1,m} + s_{2,m} * h_{u2,m} + \dots \\ &\quad + s_{u-1,m} * h_{(u-1)u,m} + \eta_{u,m}. \end{aligned} \quad (2.2)$$

The received signal of N_1 is then sent through the EC to cancel out the local echo signal and is shown in [Equation 2.3](#),

$$r_{1,m} - s_{1,m} * w_{1,m} = s_{2,m} * h_{12,m} + s_{3,m} * h_{13,m} + \dots + s_{u,m} * h_{1u,m} + \eta_{1,m}, \quad (2.3)$$

where $w_{1,m}$ denotes the estimate echo channel response by the EC and ideally, $w_{1,m} = h_{11,m}$. The outputs of all receivers of N_1 are then sent through the despreader and RAKE receiver for signal filtering, where the final received signal from N_2 is shown in [Equation 2.4](#). Notice that $y_{12,m}$ is the received signal before down-sampling phase and after the down-sampling phase, it would become,

$$\begin{aligned}
y_{12,m} &= (r_{1,m} - s_{1,m} * w_{1,m}) * c_{2,m} * h_{12,m} \\
&= y_{12,m} * h_{12,n} * h_{12,m} + y_{13,m} * h_{13,m} * c_{2,m} * h_{12,m} + \dots \\
&\quad + y_{1u,m} * h_{1u,m} * c_{2,m} * h_{12,m} + \eta_{1,m} * c_{2,m} * h_{12,m}.
\end{aligned} \tag{2.4}$$

From the above derived equations, it is not difficult to observe that $y_{13,m} * h_{13,m} * c_{2,m} * h_{12,m} + \dots + y_{1u,m} * h_{1u,m} * c_{2,m} * h_{12,m} + \eta_{1,m} * c_{2,m} * h_{12,m}$ can be regarded as an unwanted, noise-like signal for $y_{12,m}$ and thus, could be denoted as $\delta_{2,m}$. Hence, $y_{12,m}$ can be treated as $y_{12,m} = y_{12,m} * h_{12,m} * h_{12,m} + \delta_{2,m}$. Since $h_{12,m} * h_{12,m}$ is ideally 1, hence we have $y_{12,m} = y_{12,m} + \delta_{2,m}$. Similar procedure can be applied to $y_{13,m}$ till $y_{1u,m}$. Finally, $y_{12,m}$ would be sent through a quantizer and a down-sampler and becomes the final received signal $\hat{b}_{2,n}$. Similar procedure is expected for $y_{13,m}$ to $y_{1u,m}$.

The final received signals $\hat{b}_{2,n}$ to $\hat{b}_{u,n}$ can be either the designated signals to N_1 or the relay signals that utilize N_1 as a relay and will be sent after reprocessed by N_1 and the node architecture remains the same for both circumstances. The number of receivers within one node is flexible and can be adjusted based on demands but should be within the capacity boundary mentioned in the paper written by Viveck and Jafar [10] where the capacity of a network can be described as

$$C(\text{SNR}) = d \log_{10}(\text{SNR}) + o(\log_{10}(\text{SNR})), \tag{2.5}$$

where d is the number of degrees of freedom of the network, little o notation indicates $\log_{10}(\text{SNR})$ grows much faster than $o(\log_{10}(\text{SNR}))$ and C is the capacity of a network as a function of the signal-to-noise ratio (SNR), where $\text{SNR} = P_s/P_n$. P_s denotes average power of the signal and P_n denotes the average power of the noise. When SNR is high, $o(\log_{10}(\text{SNR}))$ becomes negligible in comparison to $\log_{10}(\text{SNR})$. From the paper written by Cadambe and Jafar [17], d of a full-duplex communication network

is lower bounded and upper bounded, according to [Equation 2.6](#),

$$\frac{u(u-1)}{2u-2} \leq d \leq \frac{u(u-1)}{2u-3}, \quad (2.6)$$

where u is the number of users. Hence, the capacity of a full-duplex network is bounded and any improvement would end up into interference alignment [\[17\]](#).

2.2 Circulator Design Decisions

2.2.1 Conventional Circulator

The circulator, commonly seen as a three-port Y-type circulator, has long been applied to wireless communications. Two of the most common applications are duplexers and isolators. When acting as the duplexer, the three ports will be connected to a transmitter, a receiver and an antenna, respectively. The transmitter delivers power to the antenna while the antenna delivers received signal to the receiver. It is capable of controlling the direction of signal power that flows in by simply neutralizing the power on unwanted directions with matched loads. On the other hand, an isolator would need one of the ports to be a transmitter, the second port to a device with a mismatched load. A conventional Y-circulator uses the structure described in [Figure 2.3](#). It contains three symmetric ports marked as x , y and z . Either x , y and z could be used as the port due to its symmetrical design, however, the inner bias need to be carefully considered. By default, port y is isolated. Thus, the bias would be from x to z and z to y with no signal flow between port x and y . By isolating different ports, we make use of different inner bias to separate signals. In this specific case, the circulator is expected to act as the signal isolator which could separate the received signal from the transmitted signal in order to achieve full-duplex communication.

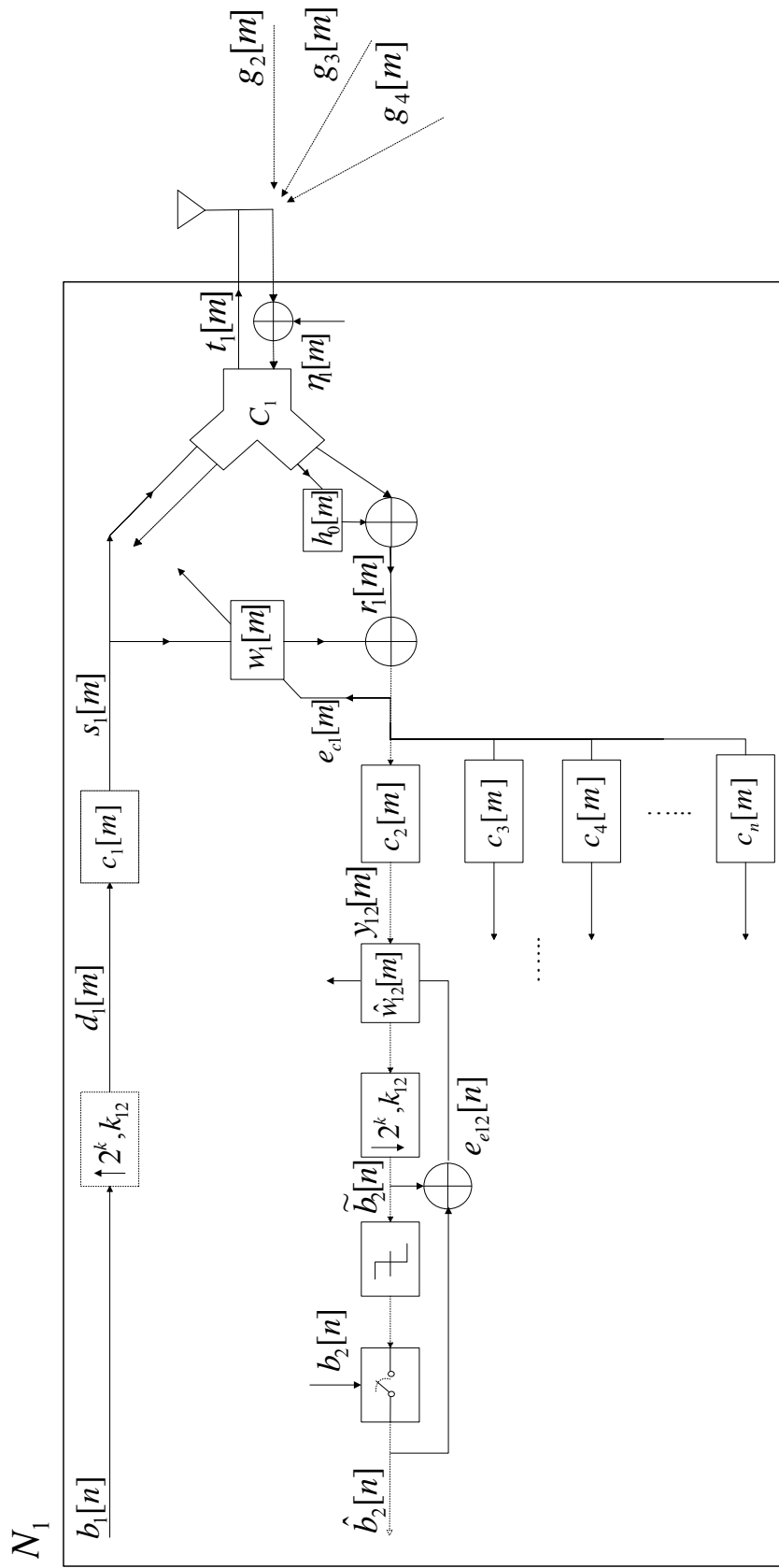


Figure 2.2: Signal Flow Diagram for a Single Node

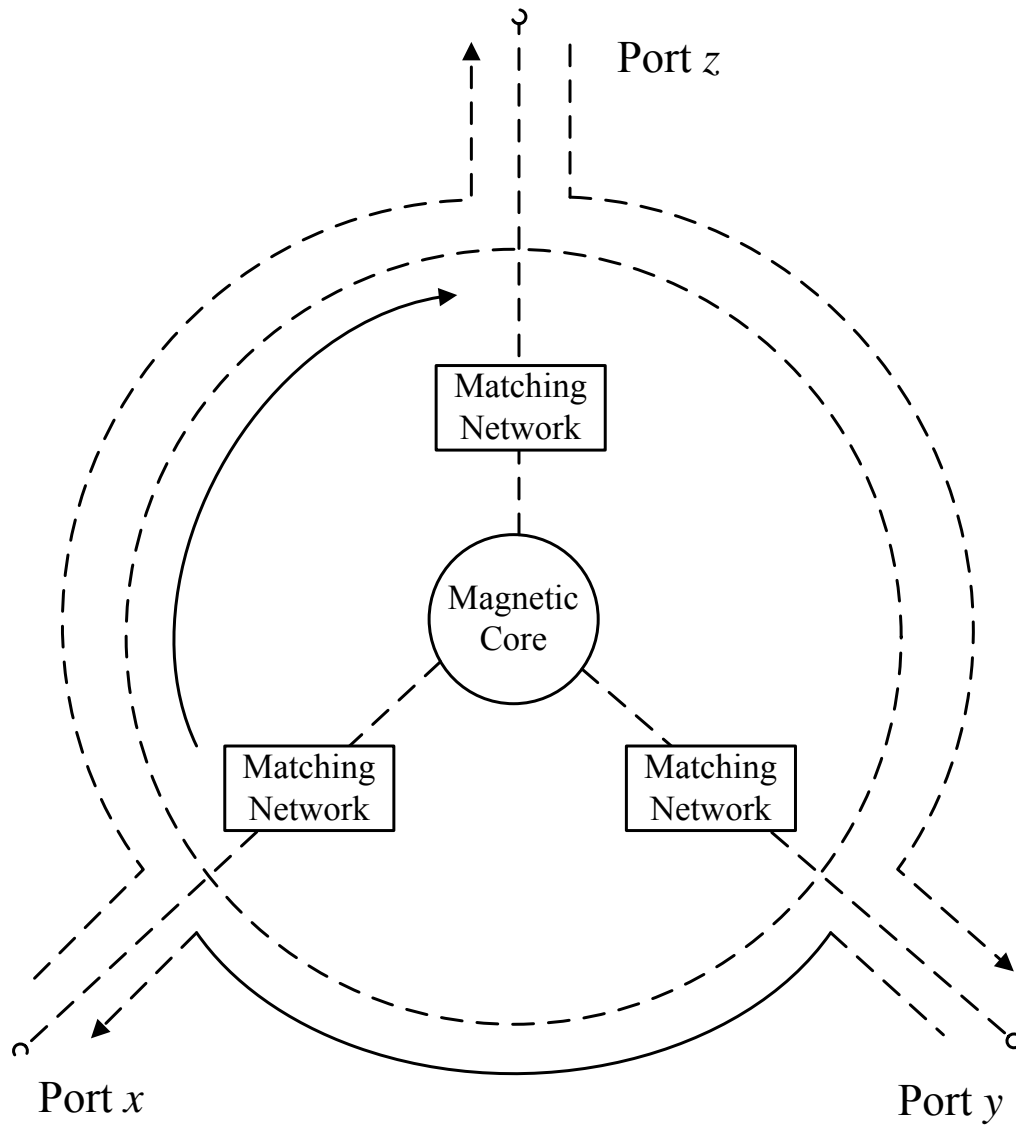


Figure 2.3: Conventional Circulator Structure

2.2.2 Circulator Requirements

The reason for implementing a circulator into the design of a full-duplex communication node architecture is that existing ECs are unable to perform properly in wireless channels where the dynamic range between the echo signal and the received signals is extremely large. Normally, the echo signal is caused by the antenna reflection, which includes a strong local echo signal as well as strong multipath signals that are reflected and picked up by the receiver itself. When compared to the power level of the received signals from other nodes that experience severe channel attenuation, the power level of the echo signal, especially the strong local echo signal, is much higher. Thus, the EC is often unable to completely cancel out the echo signal due to such a high dynamic range. By applying a circulator, a co-operative echo cancellation process is expected where the circulator will isolate a portion of the local echo signal power in order to lower the power level, then the EC will perform regularly with a reduced dynamic range.

Ideally, a circulator could provide infinite isolation. However, in practice, due to the power reflectance of the matched network caused by the mismatch of the attached load and dissipation of power in the circulator, and some power is leaked to the unintended port; the performance of a practical circulator departs from an ideal circulator. The performance of a practical circulator is measured by three aspects: return loss, insertion loss, and isolation. The ratio of the input power to the reflected power is referred to as return loss. An ideal circulator has an infinite return loss since no power is reflected back while a return loss in excess of 14 dB is achievable for actual circulators [1]. In a practical circulator, a fraction of the power delivered is dissipated within the circulator, and this is measured as the insertion loss. An ideal circulator has an insertion loss of 0 dB while an insertion loss of 0.5 dB is achievable for an actual circulator [1]. In an practical circulator, a fraction of the power delivered flows into an isolation port. The ratio of the input power to the port x to power exiting port

z is called the isolation. An ideal circulator has infinite isolation while an isolation of 20 dB is good for an actual circulator [1].

2.2.3 Innovative Circulator Design

Conventionally, the matching network in the circulator is designed to minimize the reflectance of the antenna or any other devices attached to the circulator. However, in this specific case, other than the reflectance of the antenna, the limitation of the circulator is also caused by the reflectance of other device attached to the circulator. Hence, a new design of the circulator is needed. Allen et al. developed an innovative circulator canceller which applies three dependent circulators connected to each other and with a filter connected between the first and the third circulator [1]. The architecture is described in [Figure 2.4](#). The new design intends to cancel the reflected signals passively through creating a modified (modified phases and amplitudes) copy of the unwanted signal and using it against the reflected signal. The modified version of the signal is 180 degrees out of phase with the unwanted reflected signal so that the unwanted reflected signal can be canceled out.

The modification is designed to be accomplished by a linear filter. The structure has enhanced the channel isolation ability but, contrary to conventional circulators, would add another 3 dB requirement onto the transmitted power level since at circulators I and II, the transmitted signal would split into two duplicate signals with the same energy levels. However, since the filter is responsible for modifying the phase and amplitude, a time-invariant echo channel status is needed in order to obtain the best performance.

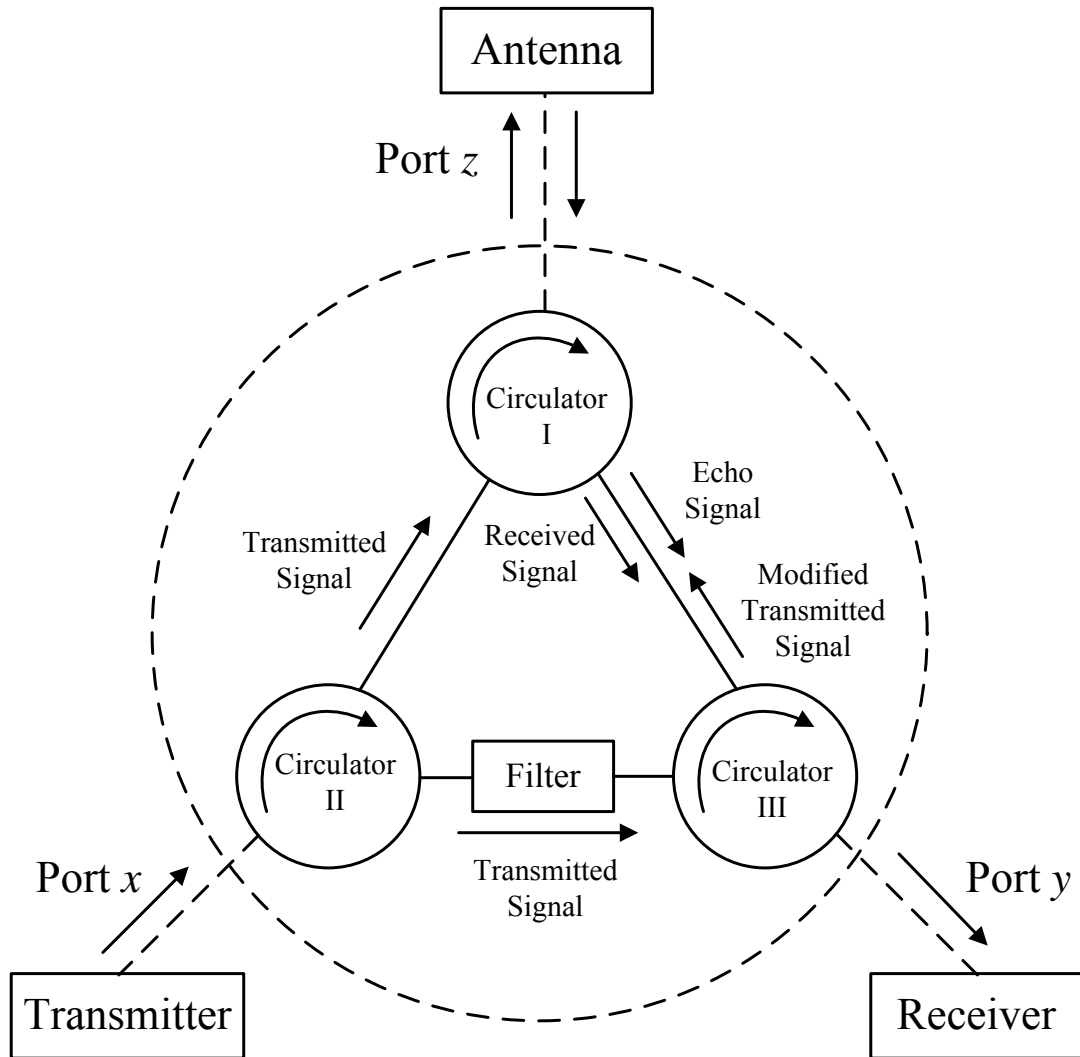


Figure 2.4: New Circulator Structure [1]

2.3 EC Design Decisions

As mentioned in the previous section, the EC, together with the circulator, is crucial in order to achieve wireless full-duplex communication. A common EC could achieve 60 to 70 dB dynamic range when it is applied to a wired system [18]. However, wireless channels have a much higher dynamic range (usually more than 90 dB), which could not be handled by the EC alone but could be achieved by the co-operative echo cancellation by the circulator and EC.

2.3.1 Conventional Linear EC

The block diagram of a linear EC is shown in [Figure 2.5](#). $b[m]$ denotes the transmitted data, $h_n[m]$ denotes the echo channel response, the block with the notation $w_n[m]$ is a linear discrete-time filter where $w_n[m]$ denotes the tap coefficients of the filter with n taps and $\hat{y}[m]$ denotes the estimate of the desired response that is optimized in the mean-squared-error sense, where $\hat{y}[m] = b[m] * w_n[m]$. While also called the echo signal, $y[m]$ denotes the signal that has gone through the echo channel. The error signal $e[m]$ denotes the difference between $\hat{y}[m]$ and $y[m]$ where $e[m] = y[m] - \hat{y}[m]$.

The error signal $e[m]$, is expected to be zero ideally, since the EC should be able to remove the entire echo. However, perfect echo cancellation is impossible to achieve in reality and thus the EC would generate the mean-squared-error, denoted as $J_y[m]$. The minimum of $J_y[m]$ is denoted as J_{\min} , or called the minimum mean-squared-error (MMSE) [19],

$$J_{\min} = E [|e[m]|^2]. \quad (2.7)$$

By applying the principle of orthogonality [19], we get

$$J_{\min} = \sigma_y^2 - \sigma_{\hat{y}}^2, \quad (2.8)$$

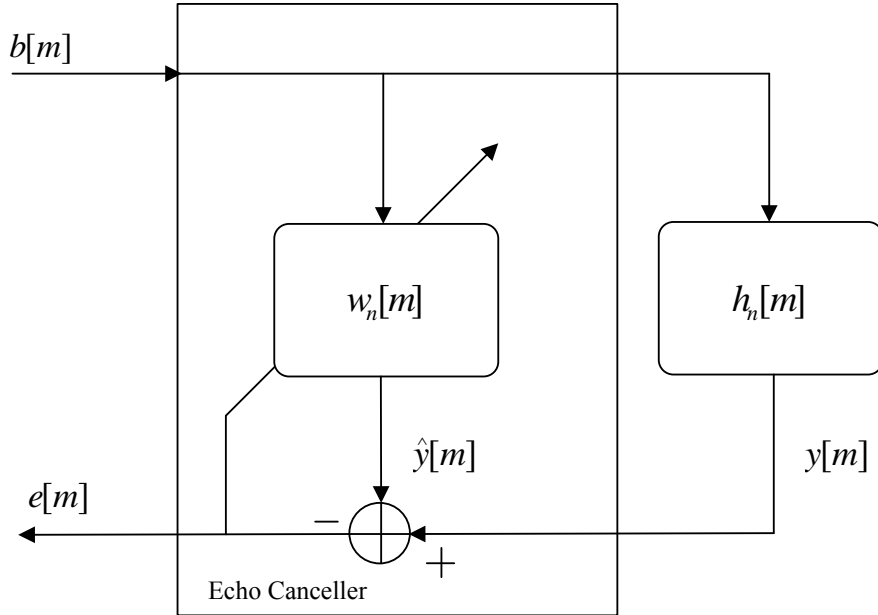


Figure 2.5: EC Structure

where σ_y^2 and $\sigma_{\hat{y}}^2$ are the variance of the desired response and the estimate separately. It is difficult to match both of the variances in practice, hence, the MMSE would not be zero.

2.3.2 EC with an On-off Switch

As for the proposed full-duplex system, the mean-squared-error would affect the performance of the RAKE receiver if it is not properly handled. From [Figure 2.1](#) we have $e_{c1}[m]$ to be the error signal or the output of the EC, where $e_{c1}[m] = s_{1,m} * \hat{w}_1[m] - r_1[m]$. Notice that $s_{1,m}$ is equivalent to the notation $s_1[m]$ and this equivalence applies to all symbols. $r_1[m]$ is the summation of the echo signal from N_1 , the received signals from other nodes $l_1[m]$ and the noise $\eta_1[m]$. From the definition of MMSE, we have

$$J'_{\min} = \sigma_{s_{2,m}}^2 + \dots + \sigma_{s_{u,m}}^2 + \sigma_{\eta_1,m}^2 + \sigma_{sre,m}^2, \quad (2.9)$$

where $\sigma_{s_{2,m}}^2$ to $\sigma_{s_{u,m}}^2$ are the variance of $s_{2,m}$ to $s_{u,m}$, which are set to be 1 assuming quadrature phase shift keying (QPSK) [4]. $\sigma_{sre,m}^2$ is the variance of the residual echo signal after the echo cancellation. $\sigma_{\eta_1}^2$ is the variance of the AWGN [4], which is $\sigma_{\eta_1}^2 = k_B T B / 2$ [4]. k_B is Boltzmann's constant, T is the room temperature in Kelvin degrees and B is the bandwidth. Thus, the MMSE for the proposed system mainly depends on the number of users in the network U . For a large number of users, the MMSE would be large and thus, the EC would consider the adaptation process incomplete and the adaptation process would still attempting to converge. While could be called *over convergence*, this unstoppable adaptation would has a severe effect on the performance of the adaptive RAKE receiver by adapting to an incorrect echo channel response. In order to minimize the effect caused by *over convergence*, the adaptation of the EC must be turned off once the correct MMSE is reached. To achieve the requirement, an EC with an on-off switch, of which the adaptation could be switched on and off due to different requirements, is needed and applied to the full-duplex system. The structure of the EC is described in [Figure 2.6](#).

Unlike a convectional EC, it has an on-off switch controlled by a detector which could detect whether the MMSE is reached or not. Once the MMSE is reached, the training process is considered terminated and the adaptation would be turned off. The MMSE is estimated and predefined in the EC at the current research stage. A more flexible and intelligent detector could be designed in the future. The training switch would remain off as long as the channels remain constant in a certain sense. If the wireless channels vary, the detector would turn on the adaptation again in order to adapt to the new channel.

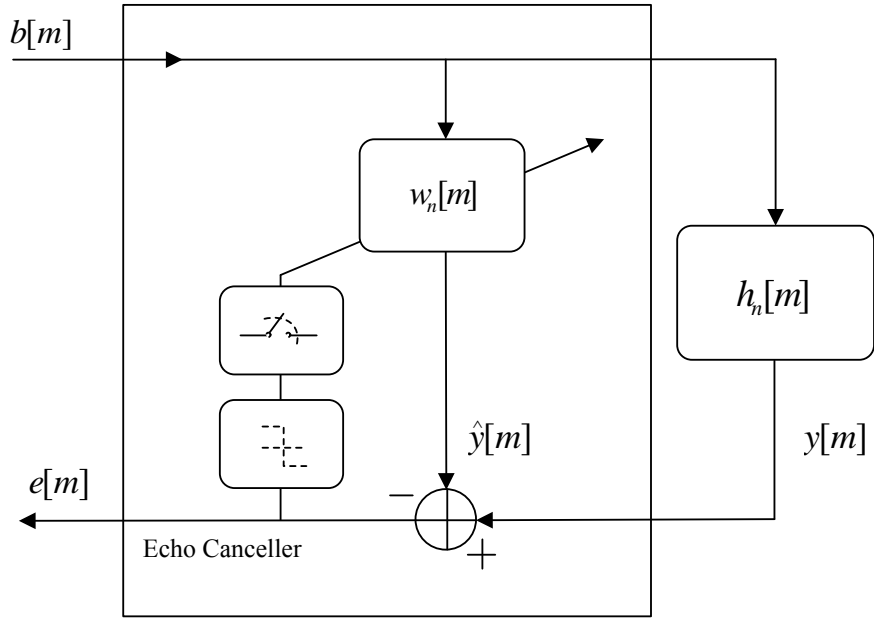


Figure 2.6: EC with an On-off Detector

2.3.3 Adaptive Algorithm

The adaptation algorithm is also a crucial factor in the convergence of the EC. The EC coefficients may be adapted using one of the variants of the recursive least square error (RLS) or the least mean-squared-error (LMS) adaptation methods [19]. The LMS method requires only $2L + 1$ complex multiplications and $2L$ complex additions per iteration but needs 2^L iterations to converge compared to L^2 complex operations per iteration but only $2L$ iterations for the RLS algorithm [19]. The above conclusion is made by assuming a stationary environment. However, while in a nonstationary environment, the LMS algorithm is found to have a superior tracking performance compared to the RLS algorithm [19]. Beyond that, the LMS algorithm is easy to implement in simulation, hence, the preference is the LMS algorithm in this specific case. The normal LMS algorithm would experience a gradient noise amplification problem when the tap-input vector is large [19], which is expected in this

specific case. The normalized LMS algorithm (NLMS) is designed to overcome this difficulty. The adaptation algorithm is described in [Equation 2.10](#),

$$\hat{\mathbf{w}}[m + 1] = \hat{\mathbf{w}}[m] + \frac{\bar{\mu}}{\|\mathbf{u}[\mathbf{m}]\|^2} \mathbf{u}[m] e^*[m], \quad (2.10)$$

where $\hat{\mathbf{w}}[m]$ indicates the tap weight vector, $\|\mathbf{u}[\mathbf{m}]\|$ indicates the norm of $u[m]$, $\bar{\mu}$ indicates the adaptation constant, $\mathbf{u}[\mathbf{m}]$ is the tap input vector and $e^*[m]$ indicates the conjugate of the error signal. The speed of adaptation would be determined by the size of $\bar{\mu}$, and it is convergent in the mean-square sense if the $\bar{\mu}/\|\mathbf{u}[\mathbf{m}]\|^2$ satisfies

$$0 < \bar{\mu} < \frac{2}{tr[R]}, \quad (2.11)$$

where $tr[R]$ is the trace of autocorrelation matrix $R = E[b[m]b^H[m]]$. Also notice that the EC is designed to adapt on the chip rate f_c and $f_c = B$. Hence, the chip rate f_c of the 5 GHz ISM band will be 111.1 MHz with guard bands based on 35% excess bandwidth raised cosine chip pulses (a detailed calculation could be found in the appendices), which indicates that the adaptation of EC will be in a relatively fast manner.

2.4 Spread Spectrum Design Decision

2.4.1 The Spread Spectrum System

One of the primary impediments of indoor high-speed wireless communications is the multipath propagation effect and ISI caused by it [4]. The solution to this impediment is diverse. Two of the most common solutions are spread spectrum and equalization at the receiver end. Spread spectrum technology exploits a pseudo-noise (PN) sequence, independent of the information data, as a modulation waveform to *spread* the signal energy over a bandwidth much greater than the signal information

bandwidth. It uses two different methods for implementation: frequency-hopping spread spectrum (FHSS) and direct-sequence spread spectrum (DSSS) [20]. A DSSS system applies a PN sequence directly on the input data to spread the transmission energy as well as the frequency, where as the FHSS system regularly hops between several predefined frequency bands. On the other hand, equalization technology applies a matched filter and several delay lines for the purpose of mitigating the ISI effect. The tap weights of the matched filter are contrary to the channel impulse response in order to be matched. Comparing both, equalization technology requires a better understanding and prediction of wireless channels while spread spectrum technology is capable of handling all sorts of channels. As Wong and Farrell suggested, spread spectrum offers a transmission waveform that exploits the properties of a spreading sequence to resolve multipath without having to resort to relatively complex solutions such as equalization [21]. Moreover, spread spectrum is capable of combating the narrowband jamming caused by varieties of factors, which could lead to a more reliable radio system. However, DSSS system performance is bounded by the properties of PN sequences. It is hard to completely resolve the effect caused by multipath in complicated indoor environment. Thus, the assistance of equalization is needed. In the proposed system, a co-operation between DSSS and adaptive equalization to overcome the ISI effect in the indoor environment is designed. In this section, only the design of the DSSS is described and discussed. Description of the equalization is described in the next section.

2.4.2 Architecture of DSSS

The block diagram shown in [Figure 2.7](#) illustrates the basic elements of a DSSS system with a binary information sequence as its input. The channel encoder and decoder apply the binary phase shift keying (BPSK) modulation to the information signal while the modulator and demodulator convolve the PN sequence with the

modulated information signal to *spread* the signal energy. In addition, the two PN sequences that interfaces with the transmitter end and the receiver end are identical. The generators generate a complex-valued PN sequence, which is impressed on the transmitted signal at the modulator and removed from the received signal at the demodulator. Also, synchronization of the PN sequence generated at the receiver end with the PN sequence contained in the incoming received signal is crucial to the DSSS system due to the demodulation requirement. One of the methods to achieve synchronization is by transmitting a high reliability fixed PN sequence to the receiver prior to the transmission of information. Once the synchronization is established, the transmission of information may commence. Another way of synchronization would be through the local clock that is contained in each of the nodes. These clocks could be synchronized through an accurate clock with a precise oscillator.

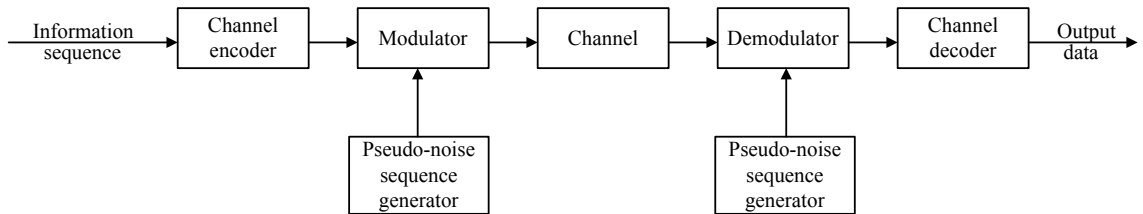


Figure 2.7: Model of Direct-Sequence Spread Spectrum

Interference is introduced while transmitting the DSSS signal through the channel. Its characteristics are heavily dependent on its origin and it can be categorized as being either broadband or narrowband relative to the carrier bandwidth, and either continuous or discrete in time [4]. In the proposed system, the interference is mostly from the channel noise and the information-bearing signals from other nodes, which can be all treated as AWGN.

An important DSSS parameter is the processing gain, which could be expressed as $PG_{dB} = 3k$ for BPSK, where PG_{dB} denotes the processing gain of the DSSS system and k is the spreading factor exponent of $K = 2^k$ [4]. The derivation of this equation

is shown in [Appendix A](#). The processing gain is an indication of the level of noise and interference for a certain DSSS system. It can also be considered as the amount of power enhancement of the information sequence. It is obvious that large amount of spreading leads to better performance, high robustness against interference but will occupy more bandwidth or lower the bit rate. Due to this trade-off, the choice of spreading factor exponent k is crucial. The determination of the spreading factor exponent k mainly depends on the channel attenuation and system requirements.

2.4.3 PN Sequence Generation

The performance of the DSSS system depends to a large extent on the PN sequences. Since in the proposed system, each code is designed to be designated an individual globally unique identification code as mentioned in [chapter 1](#), expandable spreading code families with perfect orthogonal property between each code are needed. Long pseudo-randomly generated spreading codes approach perfect autocorrelation and cross correlation properties and are expandable. However, practically it is awkward to generate long pseudo-random codes. Thus, a pseudo-random code family with an expandable property is needed. The most well-known PN sequences are the maximum-length shift-register sequences [4]. They are generated by an m -tap shift register with linear feedback as illustrated in [Figure 2.8](#).

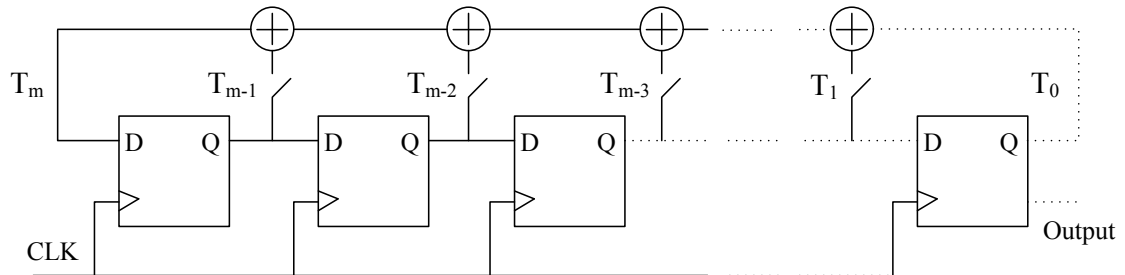


Figure 2.8: PN Sequence Generator

The tap coefficients of the shift register are selected from prime polynomials with degree m . The generated sequences, called m sequences, have a length of $n = 2^m - 1$. The m sequences have a desired periodic property and contain 2^{m-1} ones and $2^{m-1} - 1$ zeros. An advanced version of m sequences is called Gold sequences [4], which contains a good cross correlation property as well as the same autocorrelation property. Gold sequences are desired for multiple user applications such as Code-Division-Multiple-Access (CDMA) technology. It is generated by applying two shift registers with each of the two using a carefully selected polynomial, which will be discussed further in chapter 3. The sequence will be generated through the combination of the outputs from these two shift registers, as shown in Figure 2.9.

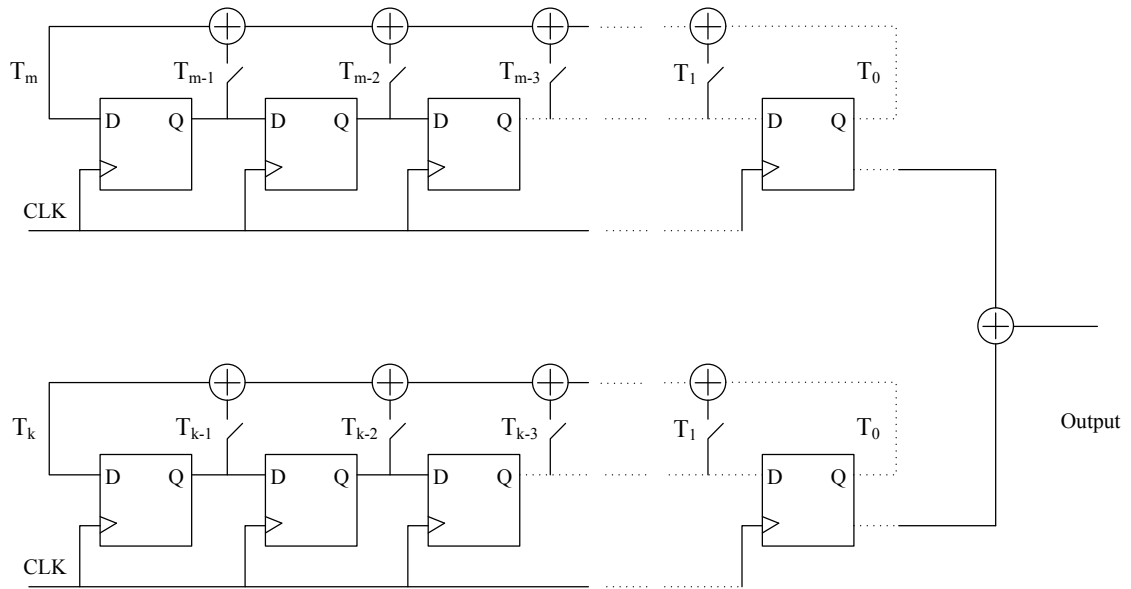


Figure 2.9: Gold Sequence Generator

Another possible candidate of the spreading sequences for the proposed system is FH sequences. Heimiller proposed a complex code generation method which could generate sequences which contain perfect autocorrelation as well as cross correlation properties in 1960s [16]. The generation of the sequences is through rearranging the

matrix of roots of unity [22] of a chosen prime polynomial p as shown in the matrix

$$\begin{pmatrix} 1, & 1, & 1, & \dots, & 1 \\ 1, & \xi_1, & \xi_1^2, & \dots, & \xi_1^{p-1} \\ 1, & \xi_2, & \xi_2^2, & \dots, & \xi_2^{p-1} \\ \vdots & & & & \vdots \\ 1, & \xi_{p-1}, & \xi_{p-1}^2, & \dots, & \xi_{p-1}^{p-1} \end{pmatrix}$$

where ξ_p denotes the p^{th} root of polynomial p and $\xi_p = e^{-j2\pi kp}$, $0 \leq k \leq p - 1$. The position of each element in the matrix is not fixed. By switching the positions, a different matrix could be generated and hence, a different FH sequence could be generated. Notice that in order to have perfect cross correlation properties between each pair of FH sequences, the code family has to be decimated. The decimation of FH sequences will be discussed further in the next chapter.

2.5 Equalizer Design Decision

As mentioned in previous section, the proposed system is expected to experience severe ISI in the indoor transmission environment. Hence, a combination of spread spectrum and equalization is needed in the system design since the implementation of equalization would reduce the requirement of the spread spectrum component, which would allow a better transmission bit rate. One of the most common equalizer structure is the RAKE receiver where its structure is shown in [Figure 2.10](#).

$r(t)$ represents the continuous received signal, $s^*(t)$ is a copy of the expected received signal where $*$ denotes complex conjugate operation, delays τ_1 to τ_n are n different delays for n different multipath component and $w^*(t)$ is the estimated channel response and it is variable through an adaptive algorithm; The RAKE receiver consists of multiple correlators; each of these correlators is called *finger*. Within these correlators, the received signal is multiplied by time-shifted versions of a locally

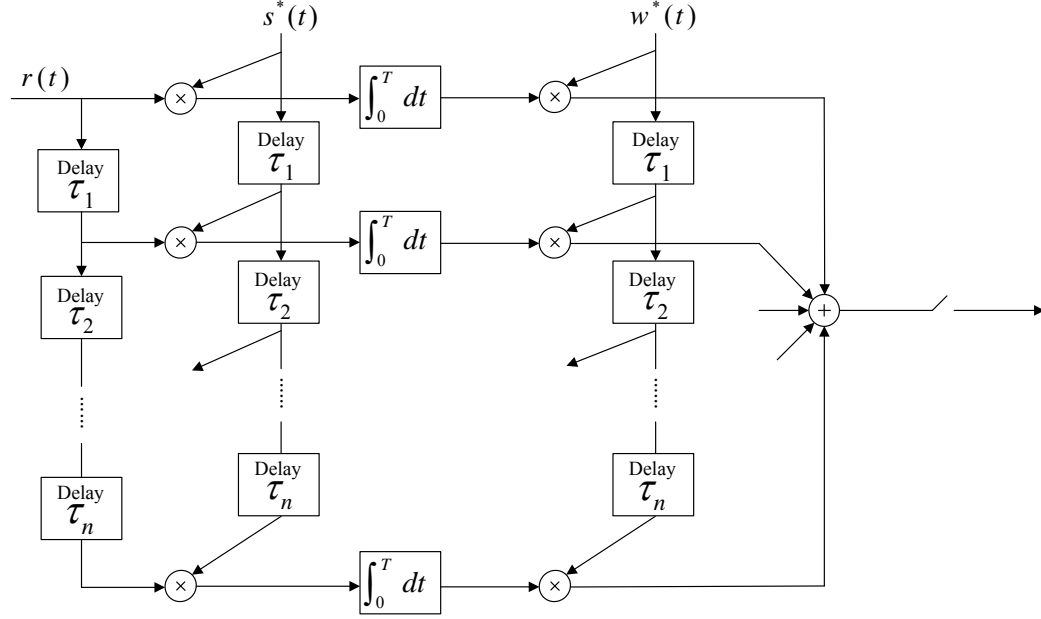


Figure 2.10: The RAKE Receiver

generated code sequence. Power is collected by the integrator through output signals from each finger and, thus, it combats the multipath fading. The number of fingers depends on the number of multipath components with significant power levels. In the proposed system, the multipath effect is mainly caused by interfering signals from other users as well as reflected signals.

The RAKE receiver in the proposed system is trained at the symbol rate f_s and with the increase in sampling rate by a factor of K while maintaining a constant bandwidth, decreases in f_s and increases the training time of the RAKE receiver will decrease the ISI. At some point, when K is large enough, the ISI would not be a concern anymore and the RAKE receiver would be unnecessary and the cost would be the reduction in transmission rate of the system.

Also notice that the architecture of the RAKE receiver is equivalent to an adaptive matched filter, however, the latter could be more easily simulated. For convenience, an adaptive matched filter is applied to replace and be equivalent to the RAKE receiver in the simulation.

Chapter 3

System Analysis

This chapter describes the system performance analysis of the system design described in [chapter 2](#), however, it is not broken down in the same manner. The first section of this chapter focusses on the system outage analysis which could show the performance of the system. The second section would show the low power consumption of the system. Notice that the design of system varies in different circumstances, thus some design trade-offs are shown in section three. Finally, in section four, we show the performance of the system using several spreading codes. As mentioned in [chapter 2](#), the system performance heavily depends on the spreading codes.

3.1 System Outage Probability

While also called outage probability, system outage probability is the probability of failing to achieve adequate reception of the signal due to, for instance, cochannel interference or multiuser interference [23]. Evaluating the probability of outage is crucial in judging the effectiveness of a certain wireless system in which the outage is affected tremendously by the signalling scheme, also called modulation scheme. An outage event is specified by a specific number of bit errors occurring in a given transmission [24]. To analyze the probability of outage, the bit error rate (BER)

of modulation schemes that are involved in the system must be analyzed.

3.1.1 Probability of Error for BPSK

For the proposed system, the signalling schemes include the source coding scheme and the channel coding scheme, where the source coding scheme is BPSK and the channel coding scheme is DSSS. As for BPSK, the probability of error function could be approximated as the M -PSK probability function as described in [Equation 3.1](#),

$$P_e = \frac{1}{\log_2 M} \operatorname{erfc} \left(\sqrt{\log_2 M} \frac{E_b}{N_0} \sin \left(\frac{\pi}{M} \right) \right), \quad (3.1)$$

where $\operatorname{erfc}(x)$ is the complementary error function and N_0 is the average baseband noise power spectral density. Hence, we have,

$$P_{e,BPSK} = \frac{1}{2} \operatorname{erfc} \left(\sqrt{\frac{E_b}{N_0}} \right). \quad (3.2)$$

The ratio between E_b and N_0 is equal to the ratio between the averaged signal power P_s and noise power P_n , assuming a constant power level for every bit of the transmitted signal.

3.1.2 Probability of Error for DSSS

On the other hand, the performance of DSSS could also be measured in terms of probability of bit error and it is given in [Equation 3.3](#),

$$P_{e,DSSS} = Q \left(\frac{1}{\sqrt{\frac{u-1}{3K} + \frac{N_0}{2E_b}}} \right), \quad (3.3)$$

where Q is the Q function [24], u is the number of different users, K is the spreading factor, E_b is the energy per bit and N_0 is the noise power spectral density. The equa-

tion above gives an irreducible error floor due to multi-user interference by assuming equal transmission power for each of the users. In practice, the near-far problem [24] would bring much difficulty into the power control of a DSSS system, thus, a more general BER calculation expression is needed. Also, from the above equation, it is clear that with the increase of u , the multi-user interference would become the dominant factor that limited the bit error rate.

3.1.3 Probability of Error for the Proposed System

Assuming the spreading factor K is 256 and the number of users u is 3, we could roughly calculate the probability of error of the proposed system by comparing the two probability of error functions and selecting the higher one. From Equation 3.3 and Equation 3.2, we could simplify the comparison to finding the greater one between $E_b/(0.005E_b + N_0)$ and E_b/N_0 , where the former is derived from the probability of error function of DSSS and the latter is derived from the probability of error function of BPSK. Notice that these factors are inversely proportional to the probability of error functions. It is obvious that the former is greater than the latter and from that we could conclude that the BER of BPSK is greater than the BER of DSSS. Hence, the error probability of the proposed system is mostly bounded by the error probability of BPSK itself. A figure that illustrates the error probability as a function of the SNR per bit for BPSK could be found in the book written by Proakis [4]. From the figure, for $P_e = 10^{-4}$, the SNR per bit is roughly 12 dB. However, this result only shows the BER before the RAKE receiver. Performance of the RAKE receiver varies due to different schemes and is usually hard to model. A specific performance analysis of DSSS with a RAKE receiver implemented in a frequency-selective fading channel could be found in the paper written by Cheun [25]. In this paper, some specific BER functions have been derived with interpath interference taken into account. These accurate BER functions could be used to describe the performance of the system

performance after the RAKE receiver.

3.2 Link Budget

3.2.1 Link Budget Analysis Criteria

The first factor that should be taken into concern for the link budget analysis is the capacity of the wireless link. As mentioned in [chapter 1](#), the proposed system is expected to be working in the 5 GHz ISM band with the central frequency 5.775 GHz and a 150 MHz bandwidth. In general, the RF power and bandwidth place an upper bound on the capacity of a communications link. The upper limit in terms of data rate is given by Shannons Channel Capacity Theorem [26]

$$C = B \log_2 (1 + \text{SNR}), \quad (3.4)$$

where C is the channel capacity in bits per second (b/s) and B is the bandwidth. Notice that this result is based on an ideal system while the bit error rate (BER) will approach zero if the data transmission rate is below the channel capacity. Practically, the degree to which a practical system can approach this limit is dependent on the modulation technique and receiver noise.

The channel noise is also intimately tied to the channel. While called AWGN or Johnson noise [4], the channel noise is mainly caused by objects that have heat, or emit RF energy, as well as interference caused by other RF devices. The noise can be calculated using

$$\eta = k_B T B, \quad (3.5)$$

where k_B is the Boltzmann's Constant, T is the temperature in Kelvin and is assumed to be room temperature (293 K). Hence, we have η to be -92.2 dBm. This is the lowest

possible amount of noise for the channel.

Another key consideration is the transmission distance. Since the signal power falls with the distance increases due to the spreading of the radio waves, it is crucial to understand the attenuation pattern in free space. The free space loss can be described as

$$L = 20 \log_{10} \left(\frac{4\pi d_0}{\lambda} \right) + 10n \log_{10} \left(\frac{d}{d_0} \right), \quad (3.6)$$

where L indicates the channel loss, d indicates the distance between the transmitter and receiver, λ indicates the wavelength of the carrier wave, d_0 is the reference distance in meters, and the path loss exponent n is 2 for free space. Notice that the above equation describes the path loss of LOS links. Due to building obstructions, such as walls and ceilings, indoor propagation losses can be significantly higher. This occurs because of a combination of attenuation by walls and ceilings, and blockage due to equipment, furniture, and even people. For example, a 2×4 wood stud wall with sheetrock on both sides results in about 6 dB loss per wall [2]. Experience has shown that LOS propagation holds only for about the first 6 m. Beyond 6 m, propagation losses indoors increase at up to 30 dB per 30 m in dense office environments [2]. The more realistic indoor propagation characteristics of the 5 GHz ISM band are measured by several researchers within different indoor scenarios [2] [27]. Some of the results are shown in Figure 3.1 and Figure 3.2, where UNII III band indicates the 5 GHz band with a central frequency of 5.775 GHz and a 150 MHz bandwidth. From the figures we can conclude that the LOS propagation characteristic of the 5 GHz ISM band has a large degree of resemblance to that of free space propagation. It is shown in Figure 3.2 that the path loss exponent n is approximately 2 for LOS measurements. To be specific, n is generally slightly less than 2 to experimental variability. The difference is mainly due to some of the energy in the 5 GHz ISM band being unable to penetrate obstacles. It is surmised that this blocked energy

is at least partly reflected, contributing to multipath gain for LOS geometries. Also from Figure 3.1, it shows that the equivalence observed in path loss exponent n in LOS geometries does not hold for NLOS paths. The path loss exponent n for a NLOS path is approximately 4.6 for the UNII band. Also notice that the standard deviation σ for the LOS and NLOS propagation are 3.00 dB and 5.01 dB, respectively.

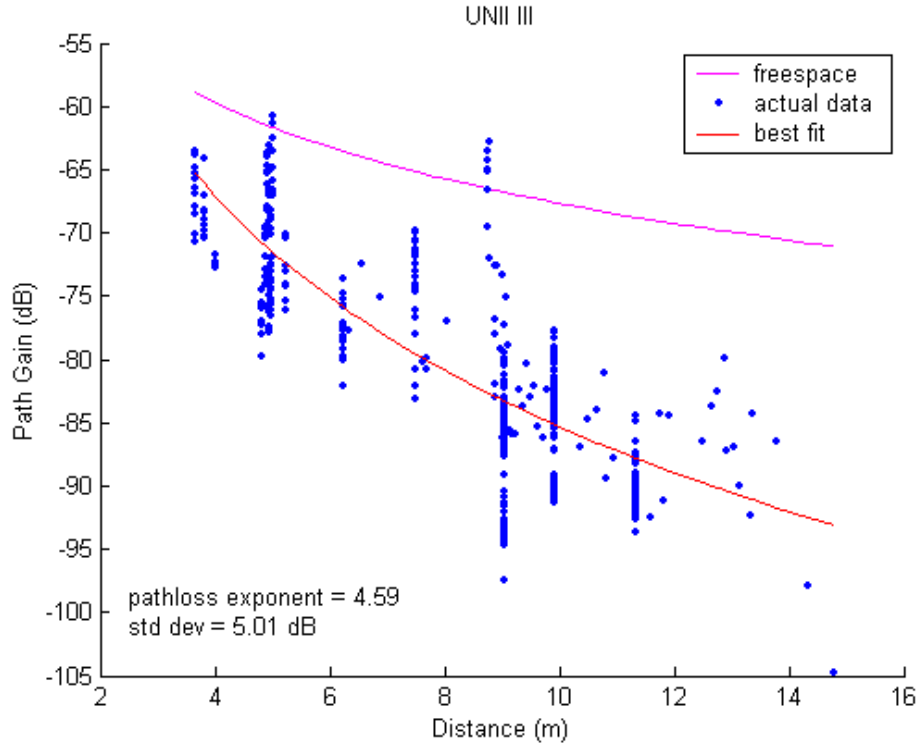


Figure 3.1: Measured NLOS path gain as a function of Distance for the 5 GHz Band [2].

The next crucial factor that needs careful analysis is the fade margin, the amount of extra power radiated to overcome multipath interference. While referred to as fading, the interference caused by multipath propagation would lead to unwanted signal distortion. A rare worst case occurs when waves traveling along different paths end up completely out of phase and cancel each other. One way to overcome this problem is to transmit more power, or have enough fade margin. In some cases, relocating or repositioning the antennas slightly may reduce the impact of multipath.

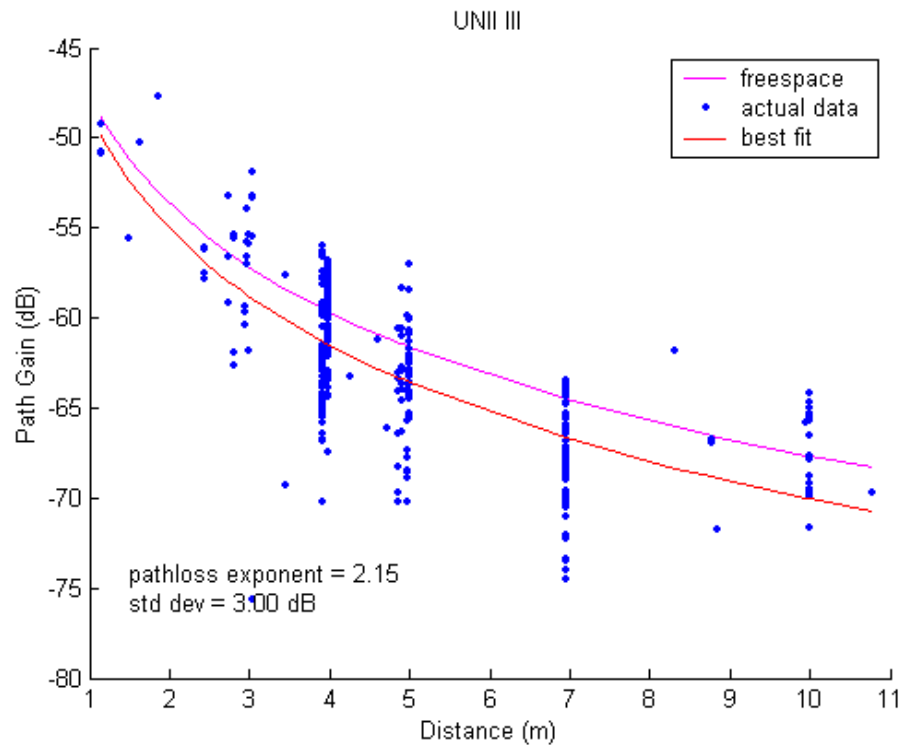


Figure 3.2: Measured LOS path gain as a function of Distance for the 5 GHz Band [2].

In an indoor environment, multipath is almost always present and tends to be dynamic (constantly varying). Severe fading due to multipath can result in a signal reduction of more than 30 dB [28]. It is therefore essential to provide an adequate link margin to overcome this loss when designing a wireless system. Failure to do so will adversely affect reliability. The exact amount of fade margin required depends on the desired reliability of the link, but a good guideline is 20 dB to 30 dB [28].

The definition of fade margin is described in [Equation 3.7](#),

$$P_f = P_r - S_i, \quad (3.7)$$

where P_f is the fade margin in dB, P_r is the received power in dB and S_i is the receiver sensitivity. The receiver sensitivity is normally defined as the minimum input signal S_i required to produce a specified SNR at the output port of the receiver and is described by

$$S_i = k_B (T_a + T_{rx}) B \frac{S_0}{N_0}, \quad (3.8)$$

where k_B indicates the Boltzmann's Constant, T_a indicates equivalent noise temperature in Kelvin of the source (e.g. antenna) at the input of the receiver, T_{rx} indicates equivalent noise temperature in Kelvin of the receiver referred to the input of the receiver, B indicates the bandwidth and S_0/N_0 indicates the SNR at the receiver end. The definition of sensitivity indicates the lowest power requirement of the signal to be recoverable by the receiver. A lower SNR requirement would lead to a lower S_i and a better sensitivity. Moreover, a lower S_i leads to a lower power requirement at the receiver end for the data signal as long as the fade margin is fixed.

Finally, the modulation scheme could effect the reliability performance of a wireless system, hence, it is necessary to consider the modulation scheme. More efficient modulation techniques such as 64-QAM require greater SNR, but less efficient

techniques such as BPSK require less SNR, and therefore are more resilient to channel noise. To help understanding, E_b/N_0 is directly related to the SNR at the receiver end. The relationship between the requirement SNR and E_b/N_0 is shown as follows

$$\text{SNR}_{dBm} = 10 \log_{10} \left(\frac{E_b R}{N_0 B} \right), \quad (3.9)$$

where R denotes the data rate, B denotes the bandwidth, E_b indicates the energy per bit and N_0 indicates the channel noise spectral density. E_b/N_0 indicates a measure of the required energy per bit relative to the noise power.

3.2.2 Specific Link Budget Analysis

Following the process of link budget analysis, we would start the analysis for the proposed system from the calculation of capacity of wireless channels. Notice that the analysis is based on the comprehensive node structure model in [Figure 2.2](#). From [Equation 3.4](#), it is clear that the desired SNR at the receiver needs to be defined and is assumed to be 20 dB. B is 150 MHz as mentioned previously. Substitute the value of SNR and B into [Equation 3.4](#), we have C equal to 661 Mb/s. Next, substitute B , k_B and T into [Equation 3.5](#), we have the channel noise η being -92.2 dBm or -122.2 dBW. Assume the indoor propagation distance d to be 30 m, we can extrapolate the channel gain A from [Figure 3.2](#) and [Figure 3.1](#). For example, the indoor channel gain of a NLOS channel at 30 m would be nearly -100 dB. As for the calculation of the receiver sensitivity S_i , we assume T_a and T_{rx} both to be room temperature and a 20 dB SNR. Thus, we have S_i to be -79 dBm.

K is assumed to be 2^8 , $G_{r,dB}$ and $G_{t,dB}$ are both 2 due to smart antennas, the channel isolation ability of the circulator C_{dB} and the echo return loss enhancement (ERLE) [29] of EC, $E_{s,dB}$, are both 40 dB and with A equal to -110 dB. Analyzing recursively, the SNR at the receiver end is assumed to be 20 dB, which indicates that the received signal needs to be 20 dB higher than the noise floor, which

leads to received signal $\hat{b}_u[n]$ having a power of -72.2 dBm after it has gone through the quantizer. Also, regarding to the fade margin P_f , the received power P_r needs to be the sum of P_f and S_i derived from Equation 3.7. Assume a 20 dB fade margin, thus, we have P_r equal to -59.2 dBm. This signal power level is brought up by the RAKE receiver and the amount could be around 10 dB as discussed in chapter 2, which leads to $y_{uu'}[m]$ being -69.2 dBm and since $y_{uu'}[m]$ is the received signal after despreader, its power level has been further brought up by the DSSS system by $3k$ dB as mentioned in chapter 2. Hence, $e_{cu}[m]$ is originally $3k$ dB lower than $y_{uu'}[m]$. In this case, $e_{cu}[m]$ is -93.2 dBm due to k being 8. Also, $e_{cu}[m]$ is called the training sequence or *error* of the EC, which is the received signal with the echo signal canceled. The power level of $e_c[m]$ is approximately the same with the power level of $r_u[m]$ except for the signal leakage problem that will cause a 3 dB power level drop. The original received signal $r_u[m]$ has experienced the channel attenuation of -100 dB, thus, the transmitted signal $t_u[m]$ would be the power level of $r_u[m]$ lowered by -100 dB and plus 6 dB (the antenna constants), which is 0.8 dBm as calculated.

On the other hand, a portion of the transmitted signal $s_u[m]$ with the power level of 0.8 dBm would leak into the receiver through echo channel $h_0[m]$ and become the echo signal. The echo signal is canceled first by the circulator. A value of C_{DB} equal to 40 dB indicates that the leaked power would be 40 dB lower than that of the transmitted signal $s_u[m]$. After canceled by the circulator, the echo signal is then processed by the EC with a value of $E_{s,dB}$ equals to 60 dB. Finally, the echo signal is reduced from 0.8 dBm to -99.2 dBm, which is below the noise floor and can be considered as noise at this point. From the above calculation, we could conclude a boundary for the transmitted signal power, where the echo signal power level could be successfully reduced below the noise floor, which is 7.8 dBm in this case. Notice that exceed the boundary transmission power would be a different circumstance in which the echo signal power level could be brought down further by the equalizer.

section, the trade-offs among some factors and how the variation of these factors would affect the system is discussed. There are four subsections where the first subsection describes the trade-off between the spreading factor exponent k and the power. The second subsection discusses the trade-off between k and the transmission distance. While also called the *degree*, k is the spreading factor exponent of the spreading code with the spreading factor $K = 2^k$. The third and fourth subsections focus on k versus the bit rate as well as k versus the EC requirement, respectively.

Resembling any other wireless system, the proposed system has the link budget that depends on multiple factors including the processing gain of the DSSS, PG_{dB} , C_{dB} , $E_{s,dB}$, the channel attenuation A and the SNR that is intended to achieve. Notice that PG_{dB} could be expressed in terms of k in [Equation 3.10](#),

$$PG_{dB} = 3k, \quad (3.10)$$

where PG_{dB} is the power level enhancement to the received signal by the DSSS system on a dB scale and the detailed derivation is shown in the appendix. Variation of the mentioned factors will cause differences in link budget calculations. A relationship between is shown in Equations 3.11 to 3.15,

$$P_{r0,dBm} = -E_{s,dB} - C_{dB} + P_{t1,dBm} \quad (3.11)$$

$$P_{r1,dBm} = 3k + G_{r,dB} + A_{dB} + G_{t,dB} + G_{e,dB} + P_{t2,dBm} \quad (3.12)$$

$$P_{r1,dBm} \geq P_{r0,dBm} + SNR_{dB} \quad (3.13)$$

$$P_{t1,dBm} = P_{t2,dBm} \quad (3.14)$$

$$P_{r1,dBm} \geq P_{f,dB} + S_{i,dB}. \quad (3.15)$$

SNR is the signal-to-noise ratio at the receiver output, $3k$ is the processing gain of the DSSS system, $E_{s,dB}$ is the ERLE, which indicates the echo cancel ability of an

EC in dB, C_{dB} is the channel isolation ability of the circulator in dB and A is the channel gain in dB. $G_{t,dB}$ and $G_{r,dB}$ are the antenna gains for the transmitter and receiver. $P_{r1,dBm}$ is the received power of N_1 and $P_{t1,dBm}$ is the transmitted power of N_1 . Similarly, $P_{r2,dBm}$ is the received power of N_2 and $P_{t2,dBm}$ is the transmitted power of N_2 . $P_{r0,dBm}$ is the echo signal power of N_1 . $P_{n,dBm}$ is the noise power level, which is -92.2 dBm based on Johnson's equation of noise.

In this section, the trade-offs are shown regarding how the proposed system has a flexible design that can be suitable for a variety of transmission environments and satisfy different system requirements. All the trade-offs could be shown by using the following two equations which denote two different transmission circumstances: firstly, if the EC and circulator are not able to bring the echo power level $P_{r0,dBm}$ down below the noise level $P_{n,dBm}$, the relationship between different factors could be described as the following equation,

$$C_{dB} + E_{s,dB} + 3k + G_{r,dB} + G_{e,dB} + G_{t,dB} + A \geq \text{SNR}_{dB}. \quad (3.16)$$

The echo signal level would be treated as the new noise floor and the equalizer would take part in the EC work. Secondly, if the EC and circulator are able to bring the echo power level $P_{r0,dBm}$ down below the noise level $P_{n,dBm}$, the relationship between different factors could be described as

$$3k + G_{r,dB} + G_{t,dB} + A + G_{e,dB} + P_{t1,dBm} \geq P_{f,dB} + S_{i,dB}. \quad (3.17)$$

The noise floor remains to be $P_{n,dBm}$ and the equalizer would not need to take part in the EC work. Notice that the receiver sensitivity $S_{i,dB}$ as well as the fade margin $P_{f,dB}$ has also limited the minimum power requirement of the system and hence, the summation of these two terms would become the new bound for the system. Also, $G_{e,dB}$ is not always a constant and depends on multiple variables such as A and

Table 3.1: Trade-off between k and $P_{t,dBm}$

P_t (dBm)	k (-)	A (dB)	SNR (dB)	G_t (dB)	G_r (dB)	P_n (dBm)
5	5	-100	20	3	3	-92.2
3.5	6	-100	20	3	3	-92.2
2	7	-100	20	3	3	-92.2
0.5	8	-100	20	3	3	-92.2
-1	9	-100	20	3	3	-92.2
-2.5	10	-100	20	3	3	-92.2

$P_{t,dBm}$. A simple approach of describing $G_{e,dB}$ is $G_{e,dB} = 110 + A + P_t$, where $G_{e,dB}$ is the required equalizer gain in dB.

3.3.1 Spreading Factor Exponent k and Power $P_{t,dBm}$

Starting from the previously derived equations in the last section, it is clear that the received signal power $P_{r1,dBm}$ must be greater than the summation of $P_{f,dB}$ and $S_{i,dB}$ as well as the summation of $P_{r0,dBm}$ and SNR. By knowing the required received power, the transmitted power $P_{t2,dBm}$ and the spreading factor exponent k could be determined. Equation 3.17 shows the relationship between $P_{t,dBm}$, k and $P_{r,dBm}$. Furthermore, $P_{t,dBm}$ is bounded by the ability of the EC and circulator. A large $P_{t,dBm}$ may contribute to combatting channel fading and thus, lead to a lower k requirement and a better bit rate. However, it will instead raise the requirement of EC and circulator since the echo will be at a relatively high power level. On the other hand, a small $P_{t,dBm}$ will lead to a requirement of large amount of spreading with a low bit rate. Table 3.1 shows the trade-off between k and $P_{t,dBm}$.

Notice that Table 3.1 shows the minimum requirements on $P_{t,dBm}$, which are derived from Equation 3.17, where the EC and circulator are able to bring the echo signal below the noise floor. From the table we could observe a 3 dB linear deduction of the minimum power requirement for an increase of k by 1. Notice that the term $G_{e,dB}$ is not always a constant. When the processing gain $3k$ is large enough to bring

Table 3.2: Trade-off between k and A_{dB}

A (dB)	k (-)	P_t (dBm)	SNR (dB)	G_t (dB)	G_r (dB)	P_n (dBm)
-92.8	3	0.8	20	3	3	-92.2
-95.8	5	0.8	20	3	3	-92.2
-96.5	6	0.8	20	3	3	-92.2
-98.8	7	0.8	20	3	3	-92.2
-99.5	8	0.8	20	3	3	-92.2
-101.0	9	0.8	20	3	3	-92.2

the received the signal up to the minimum power requirement or the multipath effect is not as much severe, $G_{e,dB}$ would be unnecessary.

3.3.2 Spreading Factor Exponent k and Channel Gain A

k is also affected by the channel gain A . For a given power level $P_{t,dBm}$, an decrease in A would cause more delay spread, hence, requires a large k to overcome the difficulties. Also, the decreased A would raise the requirement of a better EC and circulator since the dynamic range between the echo signal and the received signal has increased. Moreover, a small D requires a smaller k as well as an EC, however, in many realistic transmission environments, a relatively low A is appeared. [Table 3.2](#) shows the trade-off between k , $E_{s,dB}$, C_{dB} and A .

Notice that [Table 3.2](#) shows the minimum requirements on A , which are also derived from [Equation 3.17](#), where the EC and circulator are able to bring the echo signal below the noise floor. From the table we could also observe a linear deduction of the minimum channel gain with an increase of k by 1.

3.4 Spreading Code

One of the crucial factors that determines the performance of a DSSS system is the spreading sequences. Ideally, any pair of spreading sequences should be orthogonal within a code family so that no inter-code interference would occur during the

despreading process. Moreover, for each of the codes, they should approach the perfect periodic autocorrelation property as well as the cyclic cross correlation property since the length of the spreading code is limited. In this section, the performance of several commonly mentioned code families in the proposed system are discussed and compared. They are Gold sequences, FH sequences, and pseudo-randomly generated sequences.

3.4.1 Performance of m Sequences/Gold Sequences

Firstly, we focus on the m sequence performance. The m sequence, also called the maximum length sequence, is generated by using the linear feedback shift registers and has the periodic autocorrelation property which is the approximation of a Kronecker delta function. Notice that the m sequence generates only binary codes with a pseudo-random property, which lacks phase information. Hence, for the proposed system, two different m sequences are needed for both the phases and the amplitudes. The cyclic autocorrelation function of the m sequence is described as follows

$$\phi(j) = \begin{cases} n & (j = 0) \\ -1 & (1 \leq j \leq n - 1). \end{cases} \quad (3.18)$$

For long m sequences, the values of n are large, where $n = 2^m - 1$ is the length of the m sequence, hence, the ratio between the off-peak values of $\phi(j)$ and the peak values $\phi(j)/\phi(0) = -1/n$ is small, which indicates that the m sequences are almost ideal and perform close to the perfect autocorrelation property. However, high n values would demand large transmission bandwidth or on the contrary, cause low transmission bit rates, which could not meet the transmission requirements in some applications. On the other hand, small values of n could not deliver the perfect autocorrelation property, which would affect the proposed system performance severely.

Judging from the cross correlation property of m sequences, we could derive from the cross correlation function that m sequences exhibit some correlation. It is known that the periodic cross correlation function between any pair of m sequences of the same period can have relatively high peaks [24]. Moreover, the peak value ϕ_{max} of the cross correlation function is greater than that of the autocorrelation function. Such a property is undesirable in the proposed system since the spreading sequences must exhibit the orthogonality property to prevent interference from each other. The solution of this problem is to develop sequences with better cross correlation property. Gold sequences are the most common sequences that have better periodic cross correlations. By selecting the *preferred sequences*, Gold sequences could exhibit only three peak values denoted as $[-1, -t(m), t(m) - 2]$ where

$$t(m) = \begin{cases} 2^{\frac{(m+1)}{2}} + 1 & (\text{ odd } m) \\ 2^{\frac{(m+2)}{2}} + 1 & (\text{ even } m). \end{cases} \quad (3.19)$$

Selection of the *preferred sequences* is crucial and could be achieved through the method generated by Gold [30]. By decimating a randomly chosen m sequence with a carefully chosen decimation factor q , we could generate as many *preferred sequences* as we need. Notice that Gold sequences have the cross correlation peak value $\phi_{max} = t(m)$. Comparing this result to the lower bound of m sequences using the following equation,

$$\phi_{max} \geq n \sqrt{\frac{M-1}{Mn-1}}, \quad (3.20)$$

where $n = 2^m - 1$ and M indicates the size of the sequence set. For large n and M , the equation can be approximated as \sqrt{n} , which is $\sqrt{2^m - 1}$. From the result, we can conclude that Gold sequences exhibit a better cross correlation property than the m sequences.

3.4.2 Performance of FH Sequences

Secondly, we explore the performance of FH sequences. The reason for investigating FH sequences is because of the perfect periodic cross correlation property it has and, moreover, it is a complex sequence set. Unlike m sequences, FH sequences are generated with both the real part and the imaginary part using roots of unity of a prime number p . The complex property of FH sequences is desired in the proposed system since the bipolar sequences such as m sequences need to be assigned to distinct signals for both the real part and the imaginary part, for a single node in order to achieve the BPSK modulation, which would tighten the number of available distinct sequences within a certain sequence set. FH sequences exhibit perfect periodic autocorrelation, with the peak value $\phi_{max} = h$ and off-peak values equal to 0, where h is the number of unity roots of a prime p [16]. The cross correlation property of FH sequences varies between different sequences within a certain set, as in Sarwate's inequality

$$\frac{1}{L}\theta_c^2 + \frac{L-1}{L^2(M-1)}\theta_a^2 \geq 1, \quad (3.21)$$

where L is the period of the sequences, M indicates the size of the sequence set, θ_a and θ_c indicates the maximum value of autocorrelation and cross correlation respectively. From the inequality, we can derive that for FH sequences, the θ_c must be greater than or equal to \sqrt{L} . Hence, the best performing FH sequence set would have the lowest peak value $\theta_c = \sqrt{L}$. Notice that the sizes of the optimal sequence set are relatively small compare to that of Gold sequences, which are $\sqrt{L}/2$ and L respectively. However, the advantage of FH sequences against m sequences is that FH sequences have lower off-peak values, or called sidelobes. The N -phase FH sequence of period of N^2 has all zero sidelobes in its periodic autocorrelation [16]. The method of generating the optimal FH sequence set is described in the paper written by Alltop [31]. By

Table 3.3: Comparison of Different Spreading Codes

Criteria	Gold Sequences	FH Sequences	P-Random Sequences
Autocorrelation Peak	$\phi_{max} = n$	$\phi_{max} = h$	$\phi_{max} = n$
Cross Correlation Peak	$\theta_c = \sqrt{n}$	$\theta_c = \sqrt{L}$	-
Generation Difficulty	Medium	Hard	Easy
Family Size	Large	Small	-
Type	Real	Complex	Either

satisfying the following theorem, we could generate a distinct FH sequence set with perfect autocorrelation and cross correlation properties.

Theorem: If $(q^{-1}\mu)^2 - 1$ is relatively prime to N , then the cross correlation between the decimation of FH sequences by q and by μ has constant magnitude N . According the Sarwate's inequality, the sequences that obey the above theorem contains the optimal cross correlation property.

3.4.3 Performance of Pseudo-randomly Generated Sequences

Finally, long pseudo-randomly generated sequences exhibit the perfect periodic autocorrelation property as well as a better periodic cross correlation property. It is ideal and practically unable to achieve. Moreover, the sequences as well as the the cross correlation angle between sequences are unpredictable hence, cannot be applied to a realistic system. However, the pseudo-randomly generated sequences are perfect in the research and simulation area since they can be easily generated.

In conclusion, the [Table 3.3](#) shows a comparison of these three different codes in four different criteria including autocorrelation property, cross correlation property, generation difficulty and family size.

Notice that the cross correlation peak value of pseudo-randomly generated sequence varies, hence a dash is used to indicate the value is not a constant. Also, a dash is used to indicate that the family size of the pseudo-randomly generated sequence is unpredictable. From [Table 3.3](#), we could conclude that Gold sequences

have a bigger family size and are easy to generate comparing to FH sequences. On the other hand, FH sequences are more competitive while a complex spreading sequence is needed. As for the pseudo-randomly generated sequence, it could be easily generated and flexible but could not be used other than in the simulation.

Chapter 4

Simulation and Results

The design methodology for the proposed system is based on breaking the system down into components which could be independently designed. Since the thesis is purely research work, the verification of the entire system design is simulation based. The primary simulation and debugging tool used for this thesis was MATLAB[®] version 7. Every single component of the proposed system is integrated into a simulation program which could generate random data and send it through the system in some predefined transmission environment. By investigating the outputs at the receiver end, we could verify the system design.

In this chapter, we show some simulation results of the system described in [chapter 2](#). Firstly, we show the simulation setup as well as describe the simulation environment. The second part is focused on the results shows the system trade-offs discussed in [chapter 3](#). The third part shows the results for different spreading sequences as described in [chapter 3](#).

4.1 Simulation Setup

As mentioned in [chapter 2](#), in this thesis, we focus on the indoor transmission environment, hence, the simulation simulates mainly the indoor environment with

severe multipath propagation, strong echo paths and weaker LOS and NLOS paths compare to echo paths. Notice that in order to simplify the simulation and show a general picture of full-duplex transmission, all nodes in the simulation are considered within two dimensions. Moreover, all nodes are randomly placed with different distance between each two of the nodes. The number of nodes in the simulation are chosen to be three (N_1, N_2, N_3) so that a network with minimum size could be simulated. These three nodes are identical from each other with the same transmitter component and receiver components which are used to send and receive signals from the other nodes simultaneously.

The transmitted signals from these three nodes are defined at the very beginning of the simulation. Each signal is fixed to four randomly generated, complex bits which varies each time the simulation is initialized. As discussed in [chapter 3](#), the proposed system has restrict requirements on spreading sequences, hence, preferred spreading sequences should exhibit both good autocorrelation and good cross correlation properties. For the purpose of easy simulation, spreading sequences in the simulation are pseudo-random generated complex spreading sequences. The length of the sequences is variable and could be easily adjusted through the spreading factor exponent k .

The simulated antennas are assumed to be smart antennas which could distinguish vertical and horizontal plains. Thus, the antenna gain $G_{t,dB}$ and $G_{r,dB}$ are set to be 3 dB, respectively. Also, the antennas are assumed to have a characteristic impedance of 50Ω and followed by matching networks.

4.1.1 Channel Model

The proposed system is expected to be working in the 5 GHz UNII band with the central frequency at 5.775 GHz and a 150 MHz bandwidth. The 5 GHz band holds the advantages of a wider bandwidth, less interference than 2.4 GHz. However,

regarding such a high frequency, the wavelength λ of the 5 GHz band is relatively small which leads to more interference from the multipath propagation within an indoor environment, as mentioned in [chapter 1](#).

In the real world transmission, interference would come from not only signals that are operating at the same frequency band but also signals that are operating at the nearby frequency band, which is called overlapping. Hence, it is crucial to have a small portion of available bandwidth as guard band to prevent overlapping. The proposed system is assumed to have a raised cosine filter to shape the wave in order to minimized the ISI. Its time domain impulse response is given as follows,

$$h(t) = \text{sinc}\left(\frac{t}{T_s}\right) \frac{\cos\left(\frac{\pi\beta t}{T_s}\right)}{1 - \frac{4\beta^2 t^2}{T_c^2}}, \quad (4.1)$$

where T_s is the symbol period and β is the roll-off factor. As in frequency domain, the base band frequency response can be described in [Equation 4.2](#) [4],

$$H(f) = \begin{cases} T, & \left(|f| \leq \frac{1-\beta}{2T_s}\right) \\ \frac{T_s}{2} \left[1 + \cos\left(\frac{\pi T_s}{\beta} \left[|f| - \frac{1-\beta}{2T_s}\right]\right)\right], & \left(\frac{1-\beta}{2T_s} \leq |f| \leq \frac{1+\beta}{2T_s}\right) \\ 0, & \text{otherwise,} \end{cases} \quad (4.2)$$

where $(1 - \beta)/2T_s$ is -75 MHz and $(1 + \beta)/2T_s$ is 75 MHz since the bandwidth is 150 MHz. Also, from $T_s = KT_c$, where K is the spreading factor and T_c is the chip period, we can derive that $T_c = (1 + \beta)/KB$, where B is the bandwidth. By choosing different β as well as K , we can have different chip period T_c . From the PHD thesis written by Petersen, β is set to be 0.35 [32], which indicates 35% excess bandwidth.

For an indoor wireless communication network, node placement is complex. Nodes could be either placed within the same floor with both Obstructed Line-Of-Sight (OLOS) and NLOS or placed cross-floor. The channel measurement and

modeling could be found in the. For the OLOS path, for example, the path loss is approximately 90 dB and more than 105 dB for NLOS path when the transmitter and receiver is separated by close to 30 m [27]. The regression parameters based on the distance could be modeled as a power law with $n = 2.04$ and a standard deviation of $\sigma = 4.2$ dB for the OLOS path and $n = 2.92$ and a standard deviation of $\sigma = 3.5$ dB for the NLOS path. Moreover, when the transmitter and the receiver are located between floors, regression parameters change with $n = 3.55$ and a standard deviation of $\sigma = 1.0$ dB. For the delay spread, it is investigated in the technical report written by Cheung and Prettie [2] that the median value of the rms delay spread in OLOS is approximately 27 ns, while it increases to 32 ns in NLOS. For between-floors, the median is approximately 35 ns and the 90 percent of the signal is above 50 ns.

In the simulation, we only consider about nodes that are placed in the same floor. Also the channel model for the simulation is assumed to be a frequency selective fading multipath channel model. Hence, based on the data from the 802.11 documents [27], we could generate the channel models in the simulation by generating the exponential power delay profile (PDP) that is described as follows,

$$\text{PDP}(n) = e^{\frac{-n * T_c}{T_{pdp}}} , \quad (4.3)$$

where T_{pdp} is the delay spread. After the generation of PDP, we attach the PDP to randomly generated complex channel impulse response and add the channel attenuation A to generate the frequency selective fading multipath channel model. Notice that the impulse responses generated are random and variable each time the simulation is run.

Despite the wireless channel model, we also need to consider about the echo channel model. Since we would like to simplify the simulation as well as to explore the limitation of the system, a single coefficient channel response, 0 dB attenuation echo channel is assumed. This is a reasonable assumption since the dominant echo

signal would be the leakage signal from the inside of the node which does not fade and change phase as much as the reflected signals.

4.2 Simulation Results

4.2.1 Results for System Testing

Results shown in this subsection are mean to verify and test the system design described in [chapter 2](#). The simulation is run with a 0.8 dBm transmitted power as mentioned and the spreading factor exponent k is set to be 8. Also, the echo path is set to be a single coefficient, 0 dB attenuation path. With a randomly generated channel impulse response, the simulation is considered successful while the every component of the system meets the theoretical calculation results, that is, the EC and the circulator need to achieve 100 dB cancellation, the equalizer needs to achieve 10 dB equalization and the final power level of the received signal needs to be close to the -59.2 dBm power level. The channel gain A is -100 dB when the results are obtained and any attenuation higher than -100 dB would not generate the desired results, hence, we could conclude that -100 dB is the limit. This result mostly matches the theoretical calculation.

The trained equalizer coefficients, f_m , are shown in [Figure 4.1](#) and [Figure 4.2](#) with only results for N_2 and N_3 . This is due to the simulation is designed to simulate the wireless transmission and reception of a single node within the entire network and the single node is set to be N_1 . Hence, only the data from N_2 and N_3 is desired. In [Figure 4.1](#), the results show that the equalizer has successfully matched to the random channel impulse response while in [Figure 4.2](#), the results show the equalizer has achieved 20 dB equalization against ISI. Also, from the figure, we could observe clearly the training period of the equalizer is around 10 to 20 bits. Notice that the amplitudes of coefficients are not normalized; from the values we could observe that

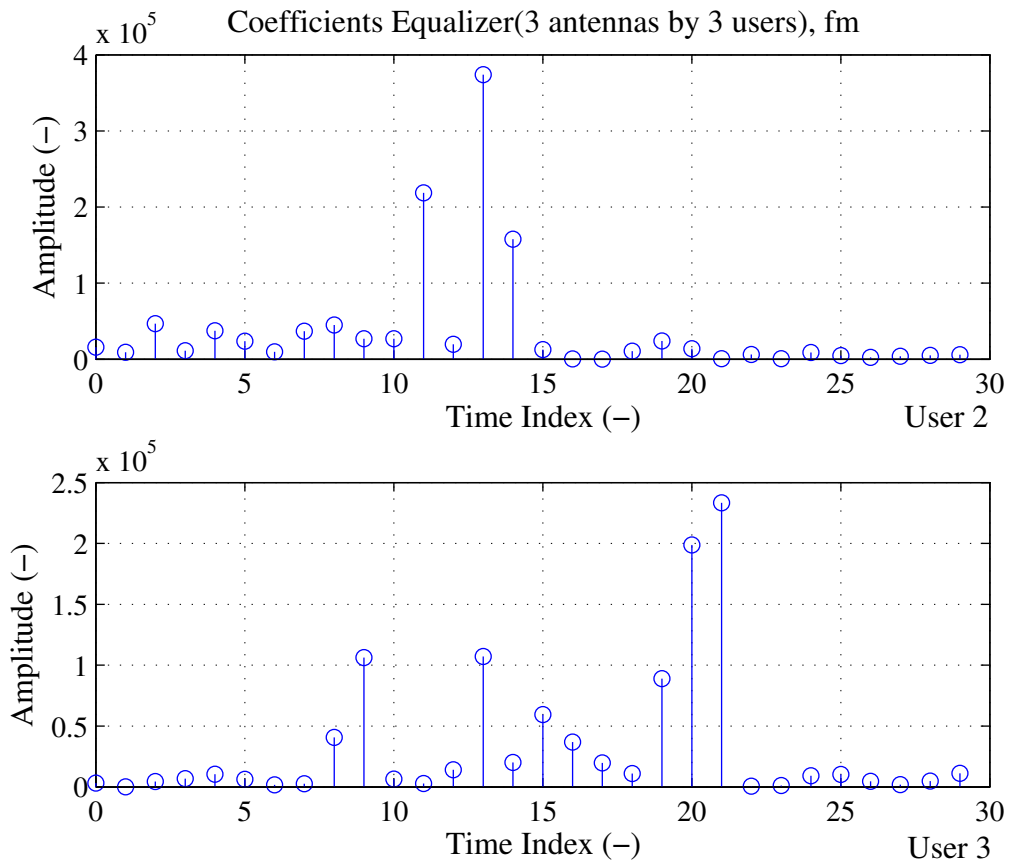


Figure 4.1: Equalizer Coefficients

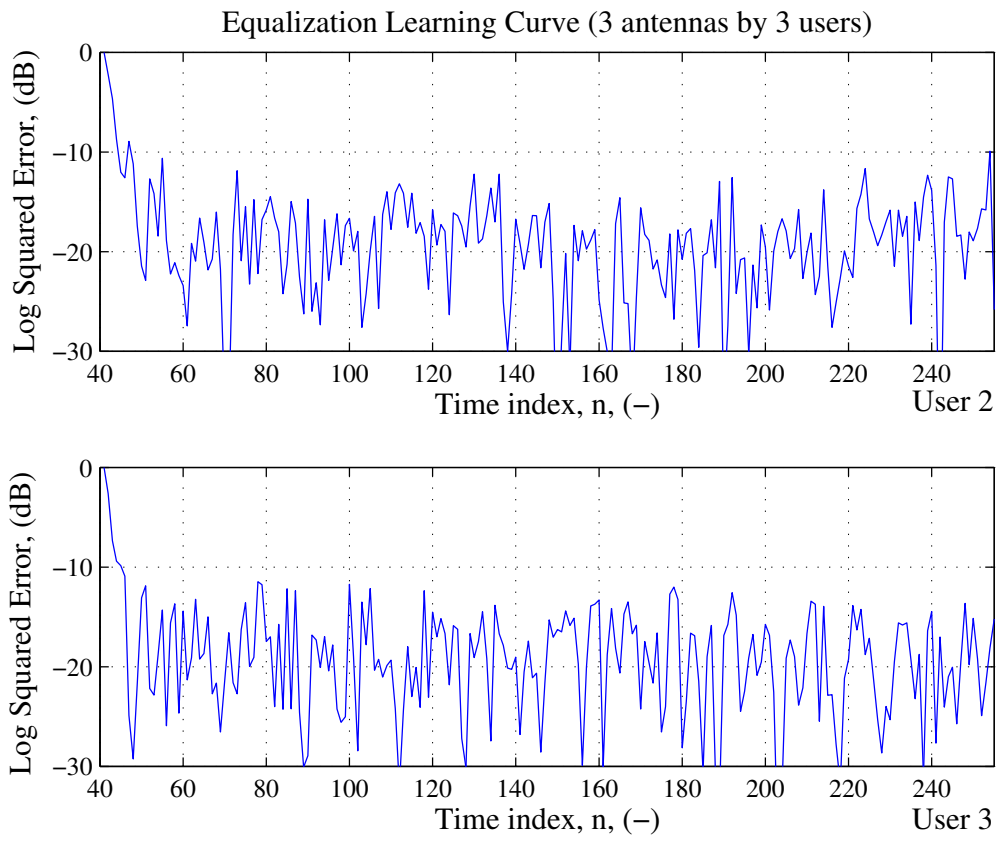


Figure 4.2: Equalizer Learning Curve

the DSSS system has successfully concentrated the energy into the data signal.

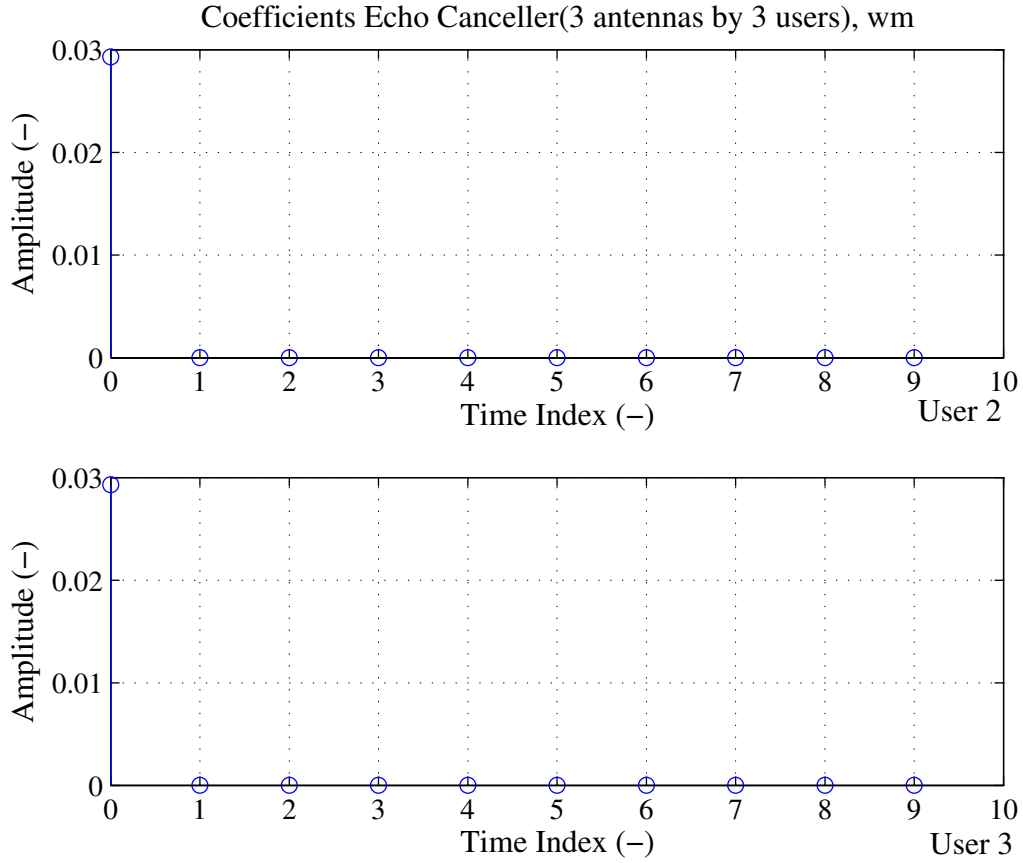


Figure 4.3: EC Coefficients

The results of the EC are shown in [Figure 4.3](#) and [Figure 4.4](#) with only results for N_2 and N_3 . In [Figure 4.3](#), the result shows the equalizer has successfully matched the echo channel impulse response while in [Figure 4.4](#), the results show the equalizer has achieved 100 dB echo cancellation. Also, from the figure, we could observe clearly the the echo cancellation begins at -40 dB since the circulator has canceled the echo signal by an amount of 40 dB and training period of the equalizer is around 250 chips, or 1 symbol. The amplitudes of EC coefficients are not normalized as well and it reflects the channel gain and DSSS energy spread from the received signal point of view.

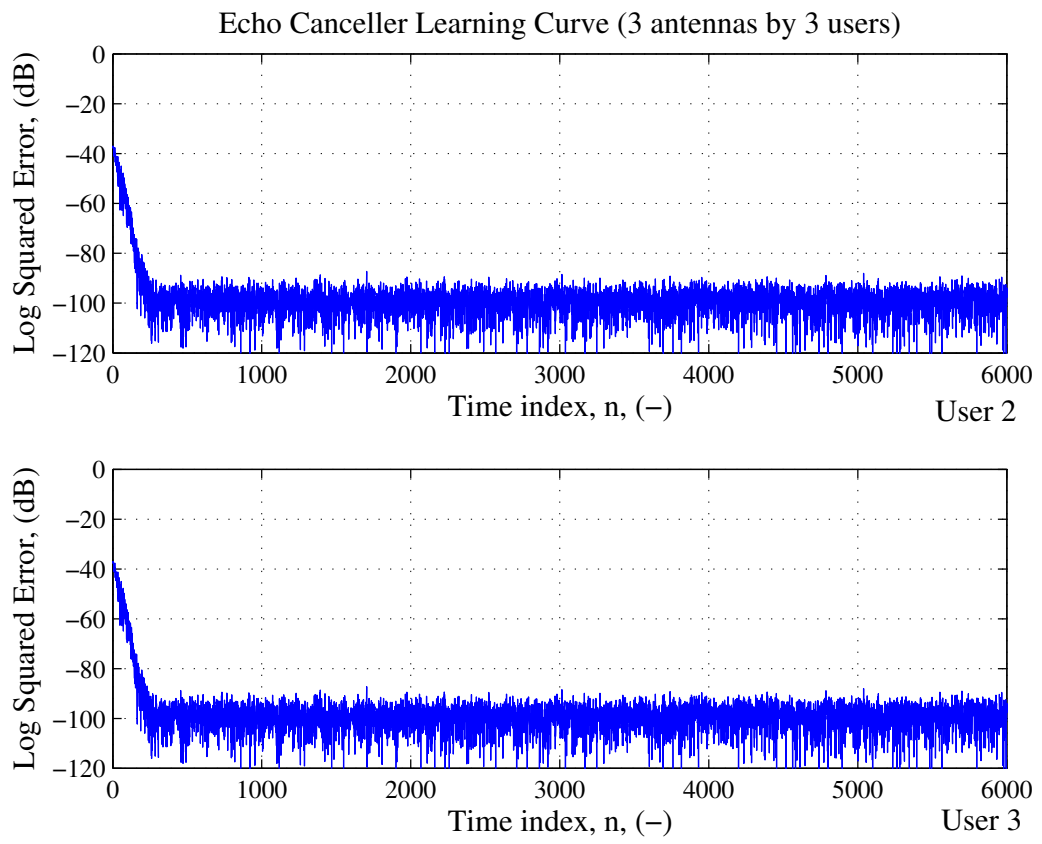


Figure 4.4: EC Learning Curve

4.2.2 Results for Trade-offs

As discussed in [chapter 3](#), the channel attenuation A is affected by the spreading factor exponent k , the ERLE $E_{s,dB}$, the circulator isolation ability C_{dB} as well as the transmitted power $P_{t,dBm}$. Once $P_{t,dBm}$, $E_{s,dB}$ and C_{dB} are fixed, A is greatly dependent on k . Extrapolation of some trade-offs between A and k is shown in [Figure 4.5](#) based on simulation results of the proposed system. In [Figure 4.5](#), trade-offs under different transmitted power $P_{t,dBm}$ are shown. From the figure we could observe that every 2 dBm rise of $P_{t,dBm}$ would reduce the requirement of k by 1 approximately for the same A . For example, if $P_{t,dBm}$ is 0.8 dBm then k needs to be greater than 11 since A equals to -100 dB, while if $P_{t,dBm}$ is 6.8 dBm then k only needs to be 8 in order to achieve the same performance. Also notice that $E_{s,dB}$ and C_{dB} are 60 dB and 40 dB respectively. With different $E_{s,dB}$ and C_{dB} , the trade-offs would be different.

In [Figure 4.6](#), trade-offs under different channel attenuation A are shown. From the figure we could observe that every 10 dB drop of A would increase the requirement of $P_{t,dBm}$ by 10 dBm approximately for the same amount of k . For example, if A is -100 dBm then $P_{t,dBm}$ needs to be greater than 8 dBm with k equals to 5. If A is -110 dB then $P_{t,dBm}$ needs to be 18 dBm in order to achieve the same performance.

Notice that from [Equation 3.15](#), we could derive a boundary of the transmitted power $P_{t,dBm}$ where the echo signal could be successfully canceled by the EC and circulator. The noise floor of the proposed system is -92.2 dBm and the required SNR is 20 dB. Also, the receiver sensitivity S_i is -79 dBm. With the increase of $P_{t,dBm}$, the power level of the echo signal after EC is increased. Once the power level is higher than -92.2 dBm, the power level would become the new noise floor. Also, from the analysis in [chapter 3](#), we know that received signal power level needs to be higher than -59.2 dBm in order to achieve a 20 dB fading margin. Hence, as long as the power level of the echo signal does not exceed -72.2 dBm, the system would be considered as working properly but with a smaller fading margin. Once the echo

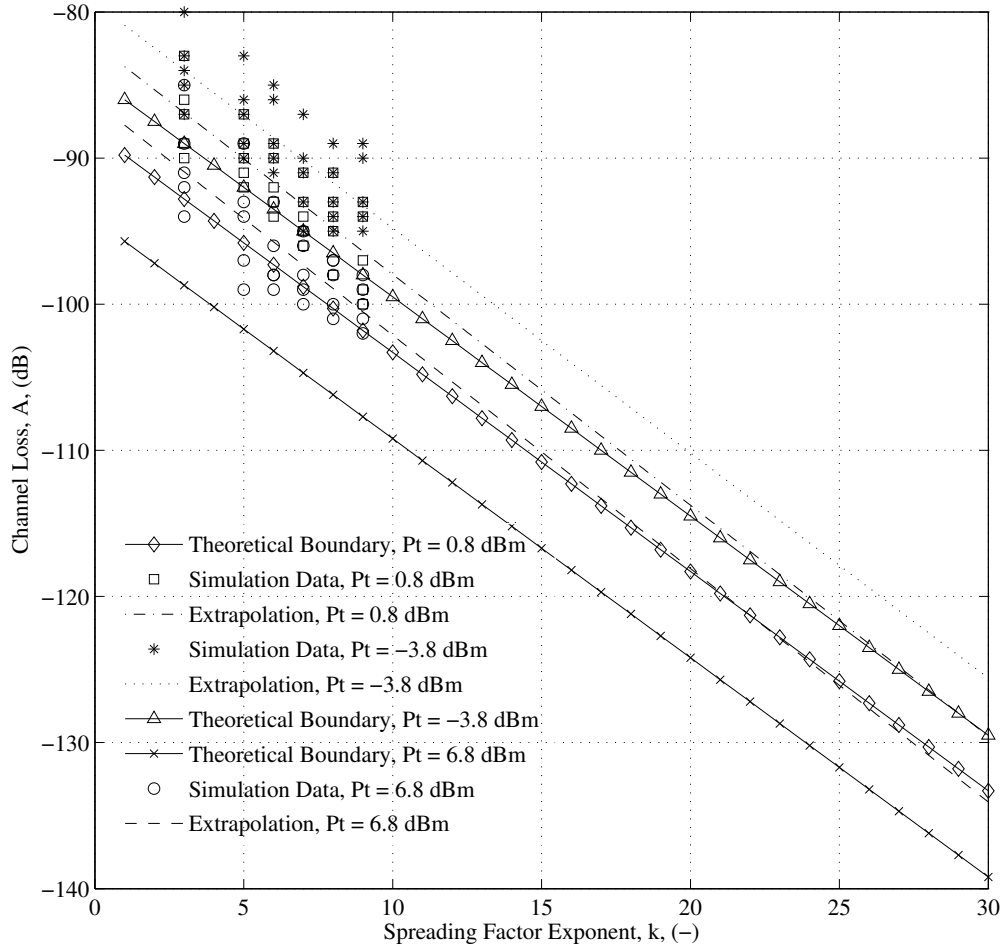


Figure 4.5: Trade-off between k and $P_{t,dBm}$

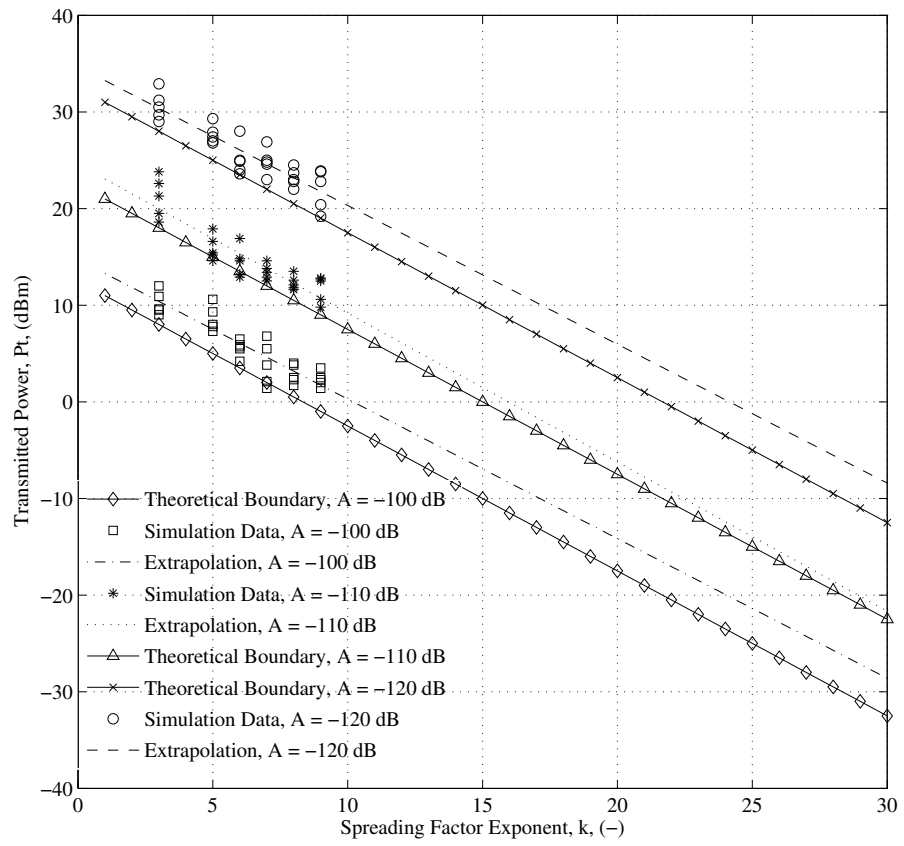


Figure 4.6: Trade-off between k and A

signal power level is higher than -72.2 dBm, the 20 dB SNR would not be achievable. Thus, according to the above analysis, at the boundary of $P_{t,dBm}$ when $E_{s,dB}$ and C_{dB} is 100 dB, echo path channel attenuation A_0 is 0 dBm. If $P_{t,dBm}$ needs to be higher than this boundary, a higher $E_{s,dB}$ and C_{dB} would be needed. In [Figure 4.6](#), results for A equal to -120 dB are obtained by assuming $E_{s,dB}$ and C_{dB} is 140 dB.

4.2.3 Results for Different Spreading Codes

In this subsection, we emphasize on showing the results of using different spreading sequences on the proposed system. The results shown here are the learning curves for both the echo cancellation and the equalization of Gold sequences and FH sequences. [Figure 4.7](#) and [Figure 4.8](#) show the results for Gold sequences are while [Figure 4.9](#) and [Figure 4.10](#) show the results for FH sequences.

The results shown here are generated with k equal to 8, A equal to -90 dB, $E_{s,dB}$ and C_{dB} equal to 60 dB and 40 dB, respectively and $P_{t,dBm}$ equals to 0.8 dBm. From [Figure 4.8](#) and [Figure 4.9](#), we observe that Gold sequences present a better autocorrelation property than FH sequences since it takes Gold sequences only approximately 250 iterations to converge while approximately 1000 iterations for FH sequences to achieve the same goal. The performance of pseudo-randomly generated sequences is omitted since they share the similar performance with Gold sequences.

This result is foretold in [Table 3.3](#), where the autocorrelation peak of Gold sequences is $\phi_{max} = n$ and the peak of FH sequences is $\phi_{max} = h$. In this case, n is 255 and h is 16 and thus, Gold sequences present a better autocorrelation property and on the other hand, FH sequences would cause residual echo signals and affect the performance of the EC.

As for the equalization convergence, Gold sequences exhibit similar property as FH sequences except that Gold sequences require less convergence time than FH sequences. Although the cross correlation property for the two sequences barely

has any difference (both equal to $2^k - 1$), This result is reasonable since the slow echo cancellation convergence for FH sequences has affected the latter equalization convergence.

Hence, the performance of equalizer depends greatly on the performance of the EC. Also, the residual echo signal would cause system outage and increase the probability of error of the entire receiver end.

This result enhanced the conclusion that for the best spreading sequence for the proposed system must have both good autocorrelation and cross correlation properties. Both of the properties should be weighted equally.

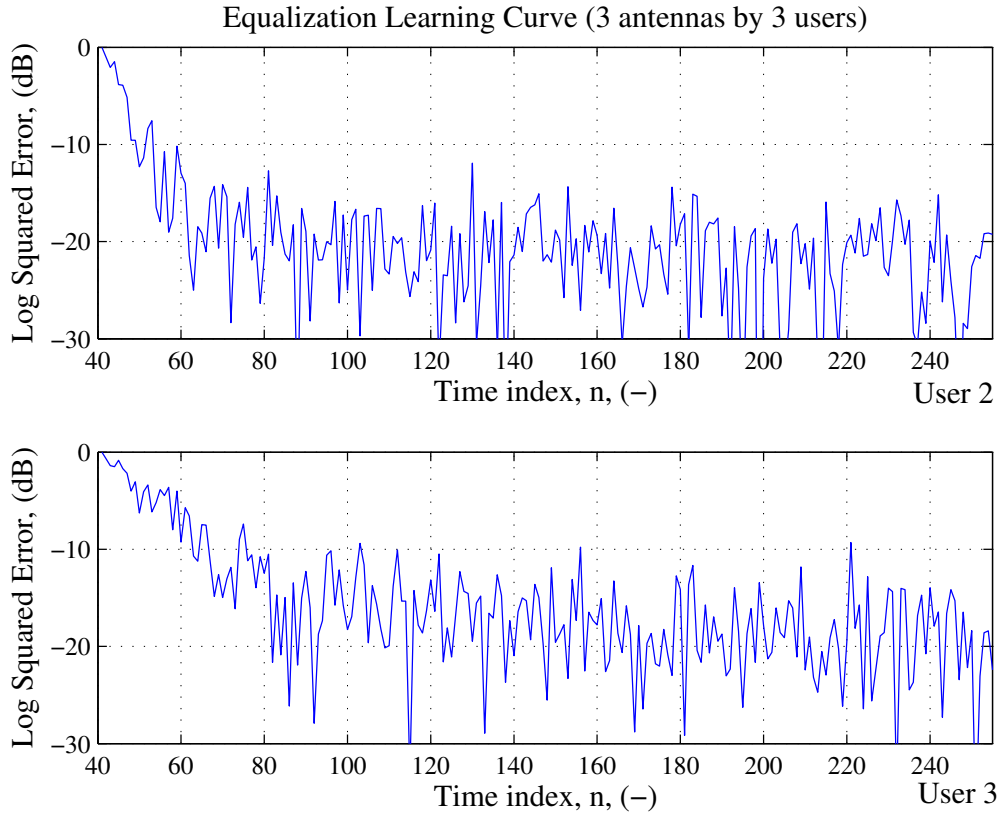


Figure 4.7: Equalization Learning Curve for Gold Sequences

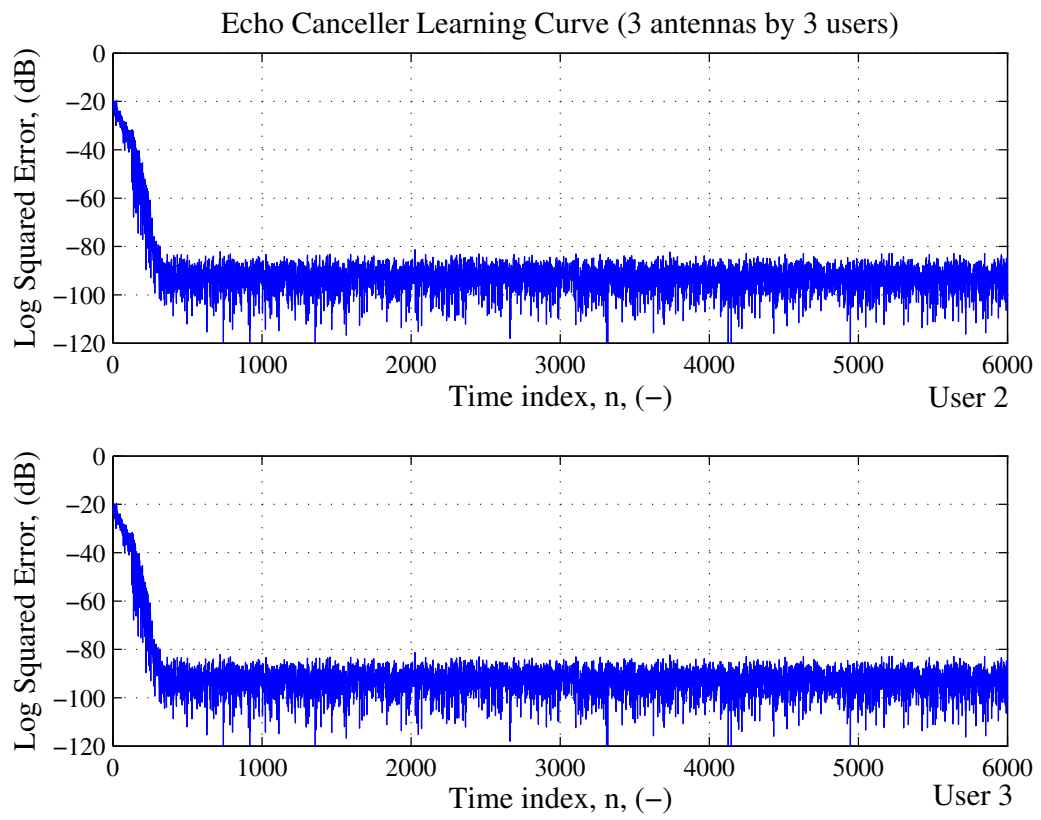


Figure 4.8: EC Learning Curve of Gold Sequences

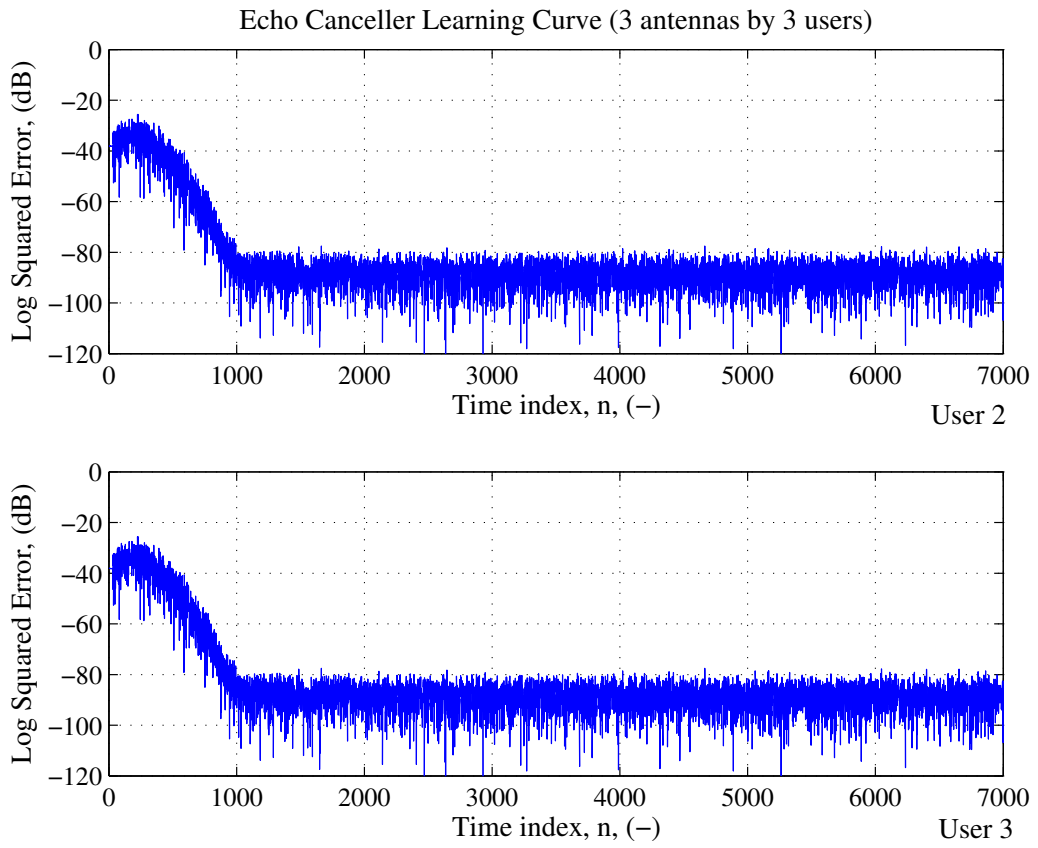


Figure 4.9: EC Learning Curve of FH Sequences

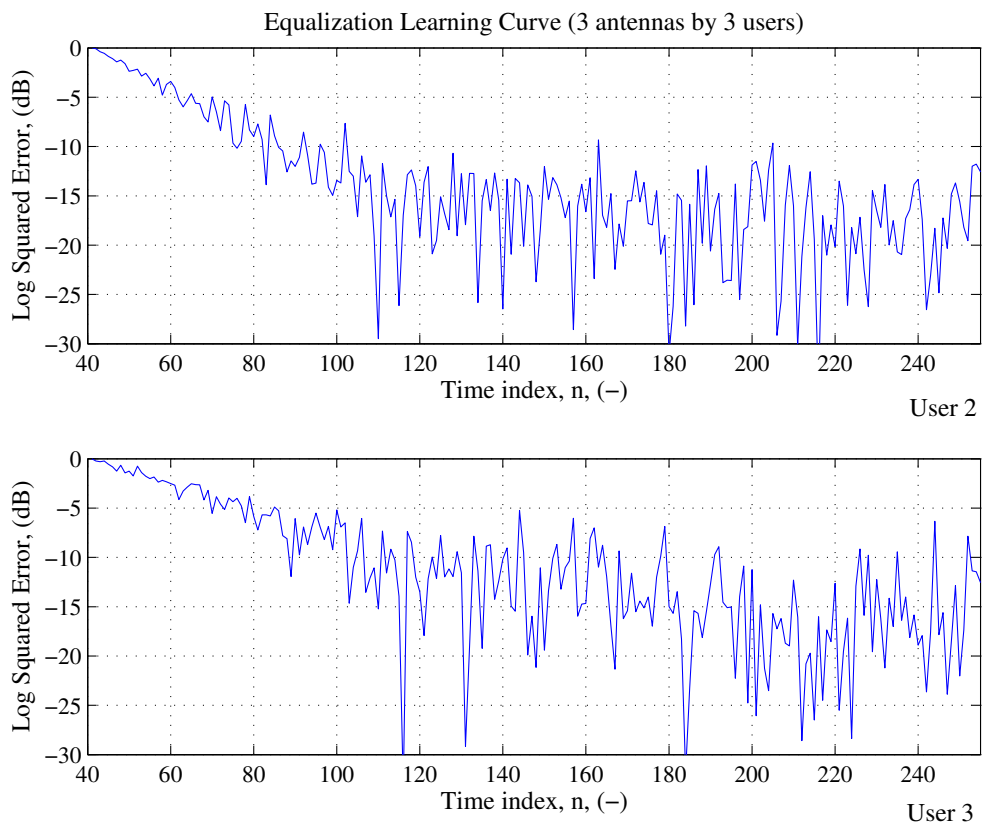


Figure 4.10: Equalization Learning Curve of FH Sequences

Chapter 5

Summary and Future Work

5.1 Summary of Work Completed

This thesis provides the physical layer design and analysis of a low-cost full-duplex co-operative communication network. The design incorporates the concept of EC, DSSS system as well as co-operative communication. The system is mainly designed for the indoor wireless transmission environment but could also be implemented in some outdoor urban area scenarios. The design process along with the analysis and simulation details of the proposed system is presented.

The node architecture of the proposed network with an EC accompanied by an innovative circulator, the DSSS technique and the RAKE receiver is designed and analyzed in the thesis. Each of the components is described and designed in details. A MATLAB[®] simulation of user signal from N_1 , N_2 and N_3 transmitting simultaneity and N_1 receiving signals from N_2 and N_3 is developed. The node architecture exhibits the desired functionality and is ready for future co-operative communication design and research.

Analysis is concentrated on trade-offs between several parameters of components of the system, system outage analysis as well as the performance comparison

of different spreading sequences. The system outage is analyzed through a simplified approximation as well as some accurate mathematical equations. Trade-offs between k , A and $P_{t,dBm}$ are analyzed with design boundaries discovered and shown for the proposed system through tables and figures. The performance of Gold sequences and FH sequences is investigated mainly from two aspects: autocorrelation and cross correlation properties, from which the conclusion that the the proposed system requires spreading sequences with good autocorrelation and good cross correlation properties.

5.2 Future Work

Due to the large size of this system, and the enormous time of comprehensive design that were required, many issues are discovered but not yet investigated in depth. Among them, the research for implementing wireless relays to the system became one of the major concerns. Either AF or DF, suggest a new relay scheme would be competitive for the system. With the help of wireless relay technologies, the proposed system is expected to have a better low-cost aspect as well as less bounded by the echo cancellation capability of the EC. Also, implementing wireless relays could effectively solve the near-far issue that has been brought up in conventional the cellular wireless communication. Secondly, accompanied with the issue of wireless relays, further effort needs to be devoted to the study of spreading sequences which could greatly affect the performance of the system. Thirdly, the communication node structure needs to be tested in a more realistic channel model with more users in order to further analyze the system performance. Finally, before any real world testing can be performed with the system radiating in the 5 GHz ISM band, there is a need to investigate and meet any requirements or limitations imposed by IEEE 802.16m standard in order to next generation network requirements.

For other future considerations, outside the initial scope of this research, would

include security and how this network connects to a larger network, such as the Internet.

Bibliography

- [1] J. C. Allen, J. W. Rockway, D. Arceo, and J. Young, “Circulator canceller with increased channel isolation.” U. S. Patent No. 7,816,995, issued Oct. 19, 2010.
- [2] D. Cheung and C. Prettie, “A path loss comparison between the 5 ghz unii band (802.11a) and the 2.4 ghz ism band (802.11b),” Intel Labs Report, Intel Labs, Intel Corporation, 2002.
- [3] A. S. Tanenbaum, *Computer Networks*. New York, NY, USA: Prentice Hall, 2003.
- [4] J. G. Proakis, *Digital Communications*. New York, NY, USA: McGraw-Hill Book Company, 1983.
- [5] J. I. Choi, M. Jain, K. Srinivasan, P. Levis, and S. Katti, “Achieving single channel, full duplex wireless communication,” *Mobile Computing and Networking (Mobicom 2010), 16th Annual International Conference on*, Sept. 20C24, 2010.
- [6] O. M. Medina, J. Vidal, and A. Agustin, “Linear transceiver design in nonregenerative relays with channel state information,” *IEEE Transactions on Signal Processing*, vol. 55, no. 06, 2007.

- [7] J. N. Laneman, D. N. C. Tse, and G. W. Wornell, "Cooperative diversity in wireless networks: Efficient protocols and outage behavior," *IEEE Transactions on Information Theory*, vol. 50, no. 12, 2004.
- [8] A. Lo and P. Guan, "Performance of in-band full-duplex amplify-and-forward and decode-and-forward relays with spatial diversity for next-generation wireless broadband," *Information Networking (ICOIN), 2011 International Conference on*, pp. 290 – 294, 26-28 Jan. 2011.
- [9] A. A. A. Haija and M. Vu, "Can half-duplex be simply derived from full-duplex communications?," *Information Theory and Applications Workshop (ITA), 2011*, pp. 1 – 4, 6-11 Feb. 2011.
- [10] V. R. Cadambe and S. A. Jafar, "Can feedback, cooperation, relays and full duplex operation increase the degrees of freedom of wireless networks?," *Information Theory, 2008. ISIT 2008. IEEE International Symposium on*, pp. 1263 – 1267, 6-11 July. 2008.
- [11] N. Serinken, B. Gagnon, and O. Erogul, "Full-duplex speech for hf radio systems," *HF Radio Systems and Techniques, Seventh International Conference on (Conf. Publ. No. 441)*, pp. 281 – 284, 7-10 Jul. 1997.
- [12] D. Guo and L. Zhang, "Virtual full-duplex wireless communication via rapid on-off-division duplex," *Communication and Control and Computing (Allerton), 2010 48th Annual Allerton Conference on*, pp. 412 – 419, Sept. 29 2010 - Oct. 1 2010.
- [13] M. Pelissier, B. Gomez, G. Masson, S. Dia, M. Gary, J. Jantunen, J. Arponen, and J. Varteva, "A 112mb/s full duplex remotely-powered impulse-uwf rfid transceiver for wireless nv-memory applications," *VLSI Circuits (VLSIC), 2010 IEEE Symposium on*, pp. 25 – 26, 16-18 Jun. 2010.

- [14] M. Omer, R. Rimini, P. Heidmann, and J. S. Kenney, “A compensation scheme to allow full duplex operation in the presence of highly nonlinear microwave components for 4 g systems,” *Microwave Symposium Digest (MTT), 2011 IEEE MTT-S International*, pp. 1 – 4, 5-10 Jun. 2011.
- [15] M. Duarte and A. Sabharwal, “Full-duplex wireless communications using off-the-shelf radios: Feasibility and first results,” *Signals, Systems and Computers (ASILOMAR), 2010 Conference Record of the Forty Fourth Asilomar Conference on*, pp. 1558 – 1562, 7-10 Nov. 2010.
- [16] R. Heimiller, “Phase shift pulse codes with good periodic correlation properties,” *Information Theory, IRE Transactions on*, vol. 07 , Issue:04, pp. 254 – 257, Oct. 1961.
- [17] V. R. Cadambe and S. A. Jafar, “Capacity of wireless networks within $o(\log(\text{snr}))$ - the impact of relays, feedback, cooperation and full-duplex operation,” *arxiv.org*, Feb., 2008.
- [18] D. D. Falconer and K. H. Mueller, “Adaptive echo cancellation/agc structures for two-wire, full-duplex data transmission,” *The Bell System Technical Journal*, vol. 58, no. 07, Sept., 1979.
- [19] S. Haykin, *Adaptive Filter Theory*. Upper Saddle River, NJ, USA: Prentice Hall, fourth edition ed., 2002.
- [20] B. Sklar, *Digital Communications*. New York, NY, USA: Prentice Hall, second ed., 2001.
- [21] K. K. Wong and T. O’Farrell, “Spread spectrum techniques for indoor wireless ir communications,” *Wireless Communications, IEEE*, pp. 54 – 63, Apr. 2003.
- [22] J. Derbyshire, *Unknown Quantity*. Washington, D.C., USA: Joseph Henry Press, first edition ed., 2006.

- [23] M. D. Yacoub, “Cell design principles,” in *The Mobile Communications Handbook* (J. D. Gibson, ed.), vol. 19, pp. 319–332, Boca Raton, USA: CRC Press, 1996.
- [24] T. S. Rappaport, *Wireless Communications*. Upper Saddle River, NJ, USA: Prentice Hall, first edition ed., 1996.
- [25] K. Cheun, “Performance of direct-sequence spread-spectrum rake receivers with random spreading sequences,” *Communications, IEEE Transactions on*, vol. 45, Issue:09, pp. 1130 – 1143, Sept. 1997.
- [26] H. Taub and D. L. Schilling, *Principles of Communication Systems*. Columbus, OH, USA: McGraw-Hill, first edition ed., 1986.
- [27] D. Dobkin, “Indoor propagation and wavelength,” RF Design, WJ Communications, 2002.
- [28] J. Zyren and A. Petrick, “Tutorial on basic link budget analysis,” Application Note AN9804, Harris Semiconductor, 1998.
- [29] K. Ho, Q. Liu, R. Rabipour, and P. Yatrou, “A new sampling of echo paths in north american networks,” *Acoustics, Speech, and Signal Processing, IEEE International Conference on*, vol. 02, pp. II809 – II812, 2000.
- [30] R. Gold, “Optimal binary sequences for spread spectrum multiplexing (corresp.),” *Information Theory, IEEE Transactions on*, vol. 13, Issue:04, pp. 619 – 621, Oct. 1967.
- [31] W. O. Alltop, “Decimations of the frank-heimiller sequences,” *Communications, IEEE Transactions on*, vol. 32, 7, pp. 851 – 853, Jul. 1984.

- [32] B. R. Petersen, *Equalization in Cyclostationary Interference*. PhD thesis, Dept. of Systems and Computer Engineering, Carleton University, Ottawa, ON, Canada, OCIEE-92-01, Jan 1992.
- [33] W. W. Peterson, *Error-Correcting Codes*. Cambridge, MA, USA: MIT Press, first edition ed., 1961.

Appendix A

Derivation of Equations

This chapter provides the derivation of processing gain PG. A more clear form of PG is shown in the thesis where PG is expressed in terms of k . The definition of the processing gain PG is defined as the ratio of symbol period and chip period [24], which can also be expressed in terms of symbol rate and chip rate. The equation is shown below,

$$\text{PG} = \frac{T_s}{T_c} = \frac{R_c}{R_s}, \quad (\text{A.1})$$

where T_s is the symbol period, T_c is the chip period, R_c is the chip rate and R_s is the symbol rate. Notice that R_s could also be expressed by R_c and the spreading factor K . For a BPSK modulated system, the bit rate R_b equals to R_c and R_b equals to $R_s K$. Hence, we have $R_s = R_c/K$. Hence, the equation [Equation A.1](#) can be expressed as

$$\text{PG} = \frac{K R_c}{R_c} = K. \quad (\text{A.2})$$

Taking log function on both side, we could derive the equation shown below,

$$\text{PG}_{\text{dB}} = 10 \log_{10} 2K = 10 \log_{10} 2^k \cong 3k. \quad (\text{A.3})$$

Also, applying the same derivation method, we could derive a general expression in terms of the spreading factor exponent k as shown,

$$PG_{\text{dB,MPSK}} = 10\log 2K = 10\log 2^k + 10\log m \cong 3k + 10\log m \quad (\text{A.4})$$

where m is the number of digits of a PSK scheme.

A.1 Derivation of Trade-off Equations

The detailed derivation of link budget equations [Equation 3.15](#) in [chapter 3](#) is shown here. A list is shown below to describe the meanings of these equations. In [Table A.1](#), it is easy to observe that the system is bounded by the echo signal power level as well as the receiver sensitivity plus the fade margin requirement. Hence, substitute the first, second and fourth equation into the third equation in the list, we have $3k + G_{r,\text{dB}} + A_{\text{dB}} + G_{t,\text{dB}} + G_{e,\text{dB}} + P_{t1,\text{dB}m} \geq -E_{s,\text{dB}} - C_{\text{dB}} + P_{t1,\text{dB}m} + \text{SNR}_{\text{dB}m}$ and this equation could be simplified into [Equation 3.16](#). Also, substitute the second and the fourth equation into the fifth equation in the list, we have $3k + G_{r,\text{dB}} + A_{\text{dB}} + G_{t,\text{dB}} + G_{e,\text{dB}} + P_{t1,\text{dB}m} \geq P_{f,\text{dB}m} + S_{i,\text{dB}m}$, which could be simplified into [Equation 3.17](#).

A.2 Derivation of Excess Bandwidth

As mentioned in [chapter 2](#), the proposed network is designed to be worked with the 5 GHz ISM band with the central frequency at 5.775 GHz and a 150 MHz bandwidth. Also, the 150 MHz bandwidth includes guard band in order to prevent interference. In this section, derivation of the chip period T_c and chip rate R_c regarding guard band is shown.

Since the transmitted signal is convoluted with a DSSS spreading sequence of length K , hence, we have the following equation,

Table A.1: Explanation of Equations

Equations	Meanings
$P_{r0,dBm} = -E_{s,dB} - C_{dB} + P_{t1,dBm}$	The echo signal power level of user 1
$P_{r1,dBm} = 3k + G_{r,dB} + A_{dB} + G_{t,dB} + G_{e,dB} + P_{t2,dBm}$	The received signal power level of user 1
$P_{r1,dBm} \geq P_{r0,dBm} + \text{SNR}_{dBm}$	The received signal power level should be greater than the echo signal power level plus SNR
$P_{t1,dBm} = P_{t2,dBm}$	The transmitted signal power level for user 1 and 2 should be equal
$P_{r1,dBm} \geq P_{f,dBm} + S_{i,dBm}$	The received signal power level should be greater than the receiver sensitivity plus the fade margin

$$\frac{K}{2T_b} = \frac{B}{2}, \quad (\text{A.5})$$

where K is the spreading factor, B is the bandwidth and T_b is the bit period. Notice that this equation is derived for baseband. For a BPSK modulation, $T_b = T_c$. Also, we use B_{lp} to represent $B/2$, which is 75 MHz. Recall that the roll-off factor β determines the excess bandwidth of the raised cosine wave form, hence, by choosing a β value, we could achieve different guard band amount. The fourier transform (FT) pairs for the continuous signal are shown below,

$$H(f) = \int_{-\infty}^{+\infty} h(t)e^{-j2\pi ft} dt \quad (\text{A.6})$$

$$h(t) = \int_{-\infty}^{+\infty} H(f)e^{j2\pi ft} df. \quad (\text{A.7})$$

Since the transmission waveform in the time domain is raised cosine wave, hence,

applying FT to the raised cosine we have the rectangular wave form in the frequency domain. The relationship is shown,

$$\text{sinc}\left(\frac{t}{T_c}\right) \leftrightarrow T_c \text{rect}(T_c f), \quad (\text{A.8})$$

where rect is the rectangular function. From [Equation 4.2](#) we can derive the relationship between B_{lp} and β shown below,

$$B_{lp} = (1 + \beta) \frac{1}{2T_c}, \quad (\text{A.9})$$

where $B_{lp} = 75$ MHz and β is chosen to be 0.35 based on north America digital cellular operating standard [\[32\]](#), which is 35 % excess bandwidth. Hence, substitute the values into [Equation A.9](#), we have $T_c = 9$ ns and $R_c = 111.1$ MHz, which means for the proposed system, the chip rate needs to be 111.1 Mc/s to allow guard bands based on 35 % excess bandwidth raised cosine chip pulses, as discussed above.

Appendix B

MATLAB[®] Simulation Source Code

B.1 Simulation Parameter Set Up

```
/******  
* This is the parameters set up for the simulation  
* Date Created: May 30, 2011  
* Copyright Author: Zhuo Li  zhuo.li@unb.ca  
* Disclaimer:      I am not liable for damages resulting from  
*                  the use of this program.  
*****/  
  
Nbits      = 2^8      ; % (-), Number of bits  
k          = 7        ; % (-)Spreading factor exponent  
K          = 2^k      ; % (-), Up sampling factor, also spreading factor  
Nusers     = 3        ; % (-), Number of users  
Dall       = [1 1 1] ; % (-), Decoding delay, must be 0,1,2,...  
Phase      = 75*[1: Nusers] .'; % (-), Phase delay  
DownSamplePhases = (K-1) * Phase*(Phase .'); %(-), Phase delays of downsamplers  
  
SNR_Rxer_in_dB = 20      ; % (dB), Signal-to-noise ratio at receivers  
C_in_dB        = 40      ; % (dB), Ciculator capability  
Fade_in_dB     = 90      ; % (dB), Channel attenuation  
mu_ec         = 2^(-5)   ; % (-), Step size
```

```

mu_eq          = 2^(15) ; % (-), Step size
Npoints_wm     = 10    ; % (-), Number of points in w, must be 1, 2, 3, ...
Npoints_fm     = 30    ; % (-), Number of points in w, must be 1, 2, 3, ...

T              = 293    ; % (K), Temperature
B              = 150e6  ; % Passband bandwidth (MHz), 5.725 (GHz) to 5.875 (GHz)
kt             = 1.38e-23 ; % (J/K), Boltzmann constant

zltraining     = 1      ; % (-), Training switch, 1 for on
zltrainingchangetime = K*Nbits ; % (-), Training time

beta           = 0.35   ; % (-), Roll-off factor
c              = 299792458.0 ; % (m/s), Speed of light
fc             = 5.775e9 ; % (Hz), Carrier frequency ISM Band Example 5.725 5.875 GHz
W              = B/2     ; % (Hz), Lowpass filter bandwidth
TH             = (1 + beta) / K*B ; % (s), Chip period
fH             = 1 / TH   ; % (chips/s), Chip rate

Tc             = 1 / fc   ; % (s), Carrier period

fT             = fH / K   ; % (symbols/s), Symbol rate
TT             = 1/fT     ; % (s/symbol), Symbol period

Blp            = 2 * (K/(2*TT)) ; % (Hz), Total complex baseband bandwidth

lc             = c / fc   ; % (m), Carrier wavelength
lT             = c / fT   ; % (m), Symbol wavelength
lH             = c / fH   ; % (m), Chip wavelength or chiplength

Gt             = 2        ; % (-), Transmitter power gain
Gr             = 2        ; % (-), Receiver power gain
Zo             = 50       ; % (Ohms), Characteristic Impedance
Pt_dB          = 0.8     ; % (dBm), Transmitted power
Pt             = 10^(Pt_dB/10)*1e-3 ; % (W), Transmitted power
V              = sqrt(10^(Pt_dB/10)*Zo*1e-3) ; % (V), Amplitude
AntennaConstant = ( lc/(4*pi) ) * ...
                 sqrt( 2 * Zo * Gr * Gt * Pt ) ; % (V m), Antenna Constant

```

B.2 Wireless Channel Impulse Response Generation

```
/******  
* This function generates random complex channel impulse  
* response.  
* Date Created: May 30, 2011  
* Copyright Author: Zhuo Li  zhuo.li@unb.ca  
* Disclaimer:      I am not liable for damages resulting from  
*                  the use of this program.  
*****/  
  
zl_cp_oneuser;  
Npdp = 2^5;  
a = 0.1;  
Tc = 9e-9;  
Tpdp = 50e-9;  
  
gmall = [];  
hnull = [];  
  
for u = 1 : Nusers ,  
    sm = small(u, :);  
    if ( u == 1 ),  
        hn = [ randn(1,1) + 1i * randn(1,1) zeros(1, Npdp-1)];  
        gm = sqrt(Wb) * uf_conv(sm, hn) ;  
    else  
        C_fade = 10^(-(Fade_in_dB/10)) ;  
        a      = 10^(-(30/10)) ;  
  
        n = [0:(Npdp-1)] ;  
        Pn = exp(-n*Tc/Tpdp) ;  
  
        hn = sqrt(C_fade)* sqrt(a)*sqrt(Pn * 50) .* (randn(1,Npdp) + 1i *randn(1,Npdp) ) ;  
  
        Erandn = abs( hn ) .^ 2 ;  
  
        gm = uf_conv(sm, hn) ;  
    endif  
  
    gmall = [ gmall ; gm ] ;  
end
```

```
    hnal1 = [ hnal1 ; hn ] ;  
end  
  
PhnWatt = uf_powerfromsignal(hnal1(2, :), 50);  
save("-text", "hnal1", "hnal1");  
cma11 = gma11 ;
```

B.3 Simulation Driver

```
/******  
* This simulation simulates a full-duplex communication network  
* Date Created: May 30, 2011  
* Copyright Author: Zhuo Li zhuo.li@unb.ca  
* Disclaimer: I am not liable for damages resulting from  
* the use of this program.  
*****/  
  
clear ;  
clear functions ;  
  
zl_cp_oneuser ;  
  
% Circulator coefficient calculation  
Wb = 10^(-(C_in_dB/20)) ;  
Wa = sqrt( 1 - Wb^2 ) ;  
  
% Noise variance at each receiver antenna  
noimannm = kt * T * B;  
  
% Signal variance at transmitter antenna  
sigmanm = sqrt(( Pt * TT * TH ) / ( K))/ TH ;  
  
bnall = [] ;  
bDnall = [] ;  
dmall = [] ;  
c0mall = [] ;  
small = [] ;  
c0m1 = [] ;  
  
% Spreading Sequences for all users  
c0mall = zl_code(3,K,Nusers) ;  
  
%Transmitter side, Generate Nusers random signals and Spread with Nusers different spreading code.  
for u = 1 : Nusers ,  
    %Generate random signals  
    bn = ( 2*fix(rand(1,Nbits)+0.5)-1 ) + ...  
          1i* ( 2*fix(rand(1,Nbits)+0.5)-1 ) ;
```

```

% Delayed data
D = Dall(u) ;
bDn = [ zeros(1,D) bn ] ;

% Upsample
dm = reshape ( [ bn ; zeros(K-1,Nbits) ] , 1 , Nbits*K ) ;

% Fetch spread code for different signals.
cOm = cOmall(u, :) ;

% Spreading spectrum
sm = uf_conv( cOm, dm ) ;

% Circulator procedure
sm = sqrt(1/2)* V * Wa * sm ;

bnall = [ bnall ; bn ] ;
bDnall = [ bDnall ; bDn ] ;
dmall = [ dmall ; dm ] ;
small = [ small ; sm ] ;
cOm1 = [ cOm1 ; cOm ] ;
end %End of Transmitter side

% Calculate the angle between spreading codes
code1 = cOmall(1,:) ;
code2 = cOmall(2,:) ;

numerator1 = real( conj(code1) * (code2.') ) ;
magsquared1 = conj(code1) * (code1.') ;
magsquared2 = conj(code2) * (code2.') ;

cosangle = real( conj(code1) * (code2.') ) ...
           / ...
           ( sqrt (magsquared1) * sqrt(magsquared2) ) ;

% Generate angle in degree
angledegrees1 = acos(cosangle) * (180/pi)

% Channel models. Generate N users channels for signals received at user 1.

gmall = zl_channel(small, Nusers, Wb, Fade_in_dB) ;

```

```

% Complex Noise Generation
nmall = [] ;

for u = 1 : Nusers ,
    nm    = randn(1,length(gmall(1,:))) + ...
            1i * randn(1,length(gmall(1,:))) ;
    %nm    = sqrt(1/2) * sqrt(noimann) * nm ;
    nm = 3.896e-6* nm ;
    nmall = [ nmall ; nm ] ;
end

rmall = gmall + nmall ;

ymall = [] ;

%Receiver Side
wms    = [] ;
fms    = [] ;
yhatmall = [] ;
dhatnall = [] ;
emall  = [] ;
eeall  = [] ;

for u = 2 : Nusers , % The first row of the received signal matrix is echo.

%Echo Cancellation
sm    = small(1,:) ;
rm    = sum(rmall) ;

%Initialization of EC
wm    = zeros(Npoints_wm,1) ;
dvecn = wm ;
ems   = zeros(1, Nbits) ;

for i = 1 : (length(sm)-1) ,
    dvecn = [ sm(i) ; dvecn( 1 : (Npoints_wm-1) ) ] ;

    % regular FIR filter processing

```

```

% obtain filter output
yhatm = (wm .') * dvecn;

yhatms(i) = yhatm ;
em      = rm( i ) - yhatm ;
ems(i) = em ;

if i <= 40*K ,
    wm      = wm + mu_ec * em * conj(dvecn) ;
end
end

emall      = [ emall ; ems ] ;
yhatmall   = [ yhatmall ; yhatms ] ;
wms        = [ wms ; reshape(wm,1,Npoints_wm) ] ;
%End of EC

%Despreading
c0m = c0mall( u , :) ;
m0m = conj(c0m(K:-1:1)) ;
ym = uf_conv(m0m,ems) ;

ymall = [ ymall ; ym ] ; %End of Despreading

%Equalization
Nsamples = length(ym) ;

% Initialize the Equalizer
fm = zeros(1,Npoints_fm) + 1i * zeros(1,Npoints_fm) ;
Rm = zeros(1,Npoints_fm) + 1i * zeros(1,Npoints_fm) ;
Rm = [ ym(1) Rm([1:(Npoints_fm-1)]) ] ;

dn = bDnall( u , : ) ;

% Approximately pre-size the array sizes for speed
zm          = 0 * ym ;
ees         = zeros(1, Nbits ) ;
dhatns     = zeros(1, Nbits ) ;

bp_i = 0 ;

```

```

x = 1;
for m = 1 : (Nsamples-1) ,

% regular FIR filter processing
% obtain filter output
zm(m) = fm * (Rm .');

%Downsampling
DownSamplePhase = DownSamplePhases(1,u);

if ( mod(m-DownSamplePhase,K) == 0 ) ,
    dhatn      = zm(m) ;
    dhatns(x)  = dhatn ;

% adapt the filter provided the delayed data exists
if ( 1 <= (x) ) & ( (x) <= length(dn) ) ,
    % adapt the filter provided the delayed data is present
    if (dn(x) ~= 0) ,
        if ( zltraining == 1 ) ,
            ee = dn(x) - dhatn ;
        else
            dncarat = uf_qam_quantizer1(dhatn) ;
            ee      = dncarat - dhatn ;
        end
    end

D = Dall(u) ;
ees(x-D) = ee ;

    if bp_i <= 40,
    else
        fm = fm + mu_eq * ee * conj(Rm) ;
    end

    bp_i = bp_i + 1 ;

else % if (dn(x) ~= 0) ,
end

else % if ( 1 <= (x) ) & ( (x) <= length(dn) ) ,
end

```

```

x = x + 1 ;

if ( x >= zltrainingchangetime ) ,
    zltraining = 1 ; % BP never stop training
else % if ( x >= zltrainingchangetime )
    end
else % if ( mod(m-DownSamplePhase,K) == 0 ) ,
    end

% shift FIR filter state
Rm = [ ym(1+ m) Rm([1:(Npoints_fm-1)]) ] ;

end
%End of EQ

eeall = [ eeall ; ees ] ;
dhatnall = [ dhatnall ; dhatns ] ;
fms = [ fms ; reshape(fm,1,Npoints_fm) ] ;

end %End of Receiver Side

%Plotting
figure(1) ;
for u = 1 : Nusers-1 ,
    subplot(Nusers-1,1,u) ;
    grid ;
    ifm = [ 0 : (Npoints_fm-1) ] ;
    stem(ifm,abs(fms(u,:).^2),'o') ;
    title('Coefficients Equalizer(User u signal), fm) ;
end % for u = 1:Nusers-1 ,

figure(2) ;
for u = 1: Nusers-1 ,
    subplot(Nusers-1,1,u) ;

    iwm = [ 0 : (Npoints_wm-1) ] ;
    stem(iwm,abs(wms(u,:)),'o') ;

    if ( u == 1 ) ,
        title('Coefficients Echo Canceller(N antennas by N users), wm) ;

```

```

    end
end % for u = 1:Nusers ,

figure(3) ;
for u = 1 : Nusers-1,
    subplot(Nusers-1,1,u) ;
    i_se_db = 0 : (length(eeall(u, :))-1) ;
    se_db = 20 * log10(abs(eeall(u, :)) + eps) - 3 ;
    plot(i_se_db,se_db) ;
    grid;
    axis ( [ 40 (Nbits-1) -30 0] ) ;
    ylabel('Log Squared Error, (dB)') ;
    xlabel('Time index, n, (-)') ;
    if ( u == 1 ) ,
        title('Learning Curve Equalization(N antennas by N users)') ;
    end
end

figure(4) ;
for u = 1 : Nusers -1,
    subplot(Nusers-1,1,u) ;
    i_se_db = 0 : (length(emall(u, :))-1) ;
    se_db = 20 * log10(abs(emall(u, :)) + eps);
    plot(i_se_db,se_db) ;
    grid;
    axis ( [ 0 (6000) -120 0] ) ;
    ylabel('Log Squared Error, (dB)') ;
    xlabel('Time index, n, (-)') ;
    if ( u == 1 ) ,
        title('Learning Curve Echo Canceller(N users)') ;
    end
end
end

```

B.4 Simulation Parameter Set Up

```
function c0mall = zl_code(Ncode, K,k, Nusers)

/*****
* This function is able to generate four kinds of spreading code
* Date Created: May 30, 2011
* Copyright Author: Zhuo Li  zhuo.li@unb.ca
* Disclaimer:      I am not liable for damages resulting from
*                  the use of this program.
*****/

switch Ncode
    case { 1 } % Frank-Heimiller Sequence
        c0mall = [] ;
        if( Nusers <= 4),
            q = 6 ;
            for n = 1 : Nusers,
                FHN = 2*K - 1 ;
                FHiset = rootsOfUnity(FHN) ;
                FHmatrix = zeros(FHN, FHN) ;
                FHmatrix(1,:) = ones(1, FHN) ;
                FHmatrix(:,1) = ones(FHN, 1) ;
                z = 1;
                for j = 2 : FHN,
                    if (z ~= (FHN - 2^(k-2)) ),
                        rt = FHiset(z);
                    else
                        rt = FHiset(z+1);
                    end

                    for i = 2 : FHN,
                        FHmatrix(j,i) = rt^(i-1) ;
                    end

                    z = z +1;
                end

                FHsequence1 = reshape((FHmatrix),1,FHN^2) ;

                if (n == 1),
```

```

        dRep=repmat(FHsequence1,1,q);
        decimatedVersion=dRep(1,q:q:end);

    else if (n == 2),

        q = 3;
        dRep=repmat(FHsequence1,1,q);
        decimatedVersion=dRep(1,q:q:end);
        else
        q = 12;
        dRep=repmat(FHsequence1,1,q);
        decimatedVersion=dRep(1,q:q:end);
        end
    end

    FHc1c = decimatedVersion ;
    c0mall = [c0mall;FHc1c] ;

    end
else
    error('Number of users must be less than 4') ;
end

case { 2 } % Feng, Fan, Hao
if( Nusers <= 4),
    FFHc1a = [] ;
    FFHc1b = [] ;
    FFHc1c = [] ;
    FFHc1d = [] ;

    for i = 1 : K/8,
        FFHc1a = [ FFHc1a 1 1 -1i -1i 1 1 -1i -1i ] ;
        FFHc1b = [ FFHc1b 1 1 1i 1i -1 -1 -1i -1i ] ;
        FFHc1c = [ FFHc1c 1 1 -1 -1 1 1 -1 -1 ] ;
        FFHc1d = [ FFHc1d 1 1 1i 1i -1 -1 -1i -1i ] ;
    end

    c0mall = [FFHc1a ; FFHc1b ; FFHc1c ; FFHc1d] ;

else

```

```

        error('Number of users must be less than 4') ;
    end

case { 3 } % Random Codes
    if( Nusers <= 4),
        c0mall = rand_codes1(Nusers,K,4) ;
    else
        error('Number of users must be less than 4') ;
    end

    [crossCorrelation,lags]=crossCorr(c0mall(1,:),c0mall(2,:));
    plot(lags,crossCorrelation);

case { 4 } % m sequences
    if( Nusers <= 4),

        n= 8;                                %Register size for m sequence generation
        polynomial = [8 6 5 3 0];           %Polynomial m-sequence
        numOfGoldSeq= Nusers - 2;           %Number of Gold sequences to generate
        q=5;                                  %Decimation factor for preferred pair generation
        N=2^n-1;                               %Length of m-sequence

        %d and dDecimated are preferred pair (if and only if the three conditions
        %for preferred-pair generation are satisfied)
        %Generate Preferred pairs by decimation
        [d,dDecimated]=genDecimatedPNSequence([8 6 5 3 0],q);

        %Generate Gold code from Preferred Pairs
        goldSequences = zeros(2+numOfGoldSeq,N);
        goldSequences(1,:)= d;
        goldSequences(2,:)= dDecimated;

        dDecimatedShifted=dDecimated;

        for rows = 3:2+numOfGoldSeq
            goldSequences(rows,:)=xor(d,dDecimatedShifted);

            %Cyclic Shifting dDecimated by 1 bit for each Gold Sequence
            dTemp=dDecimatedShifted(end);
            dDecimatedShifted(2:end) = dDecimatedShifted(1:end-1);
            dDecimatedShifted(1)=dTemp;
        end
    end

```

```
        c0mall = ones(2+numOfGoldSeq,N) - 2 * goldSequences ;
    else
        error('Number of users must be less than 4') ;
    end
otherwise
    error('invalid value') ;
end
```

B.5 Function of Root of Unity

```
function z = rootsOfUnity(n);

/*****
*rootsOfUnity y=rootsOfUnity(x) y will be a vector of all roots
*   of unity of polynomial x.
*
* Usage example:
* polynomial = [ 1 0 1 1 ]
* rootsOfUnity = rootsOfUnity ( polynomial )
*
* This function is able to generate four kinds of spreading code
* Date Created: May 30, 2011
* Copyright Author: Zhuo Li  zhuo.li@unb.ca
* Disclaimer:      I am not liable for damages resulting from
*                  the use of this program.
*****/

assert(n >= 1, 'n >= 1');
z = roots([1 zeros(1,n-1) -1]);

end
```

B.6 Function of Convolution

```
function z=uf_conv(x,y)

/*****
* UF_CONV z=uf_conv(x,y) performs a convolution of x and y.
* It uses ffts and works on complex values.
*
* Usage example:
*     x = [ 1 -1 1 1 ] ;
*     h = [ 1.0 0.1 ;
*     y = uf_conv ( h , x )
*
* Copyright Author: Brent R. Petersen b.petersen@ieee.org
* Date Created:     January 15, 2009
* Date Modified:   March 30, 2010
* Disclaimer:      I am not liable for damages resulting from
*                  the use of this program.
*****/

x2=uf_makerow(x);
y2=uf_makerow(y);
[nx,lenx]=size(x2);
[ny,leny]=size(y2);

if (nx==1) & (ny==1),
    l2=max([lenx leny]);

    lx=2^(fix(uf_logb(lenx,2)+10*eps)+2);
    ly=2^(fix(uf_logb(leny,2)+10*eps)+2);
    l = max([lx ly]);
    z2=ifft(fft([x2 zeros(1,l-length(x2))]).*fft([y2 zeros(1,l-length(y2))]));
    z=z2(1:(lenx+leny-1));
end
```

B.7 Function of Decimated PN Sequences

```
function [pnSequence,decimatedVersion]=genDecimatedPNSequence(polynomial,decimationFactor)
```

```
/******  
* Function to generate a decimated maximal length PN sequence  
* Date Created: May 30, 2011  
* Copyright Author: Zhuo Li  zhuo.li@unb.ca  
* Disclaimer:      I am not liable for damages resulting from  
*                 the use of this program.  
*****/
```

```
q=decimationFactor;  
pnSequence=genPNSequence(polynomial);  
dRep=repmat(pnSequence,1,q);  
decimatedVersion=dRep(1,q:q:end);
```

Appendix C

Table of Irreducible Polynomials

The generation of Gold sequences as mentioned in [chapter 2](#) requires primitive polynomials, which are selected from the table of irreducible polynomials over $GF(2)$ [33], where GF is Galois field of two elements. Polynomials are represented in octal and the alphabetic characters give the meanings that are shown in [Table C.1](#). A portion of the table is shown below.

To generate the Gold sequence, we need to pick a polynomial within a certain degree. The preference of the polynomial would be primitive prime polynomials since they would have less cochannel interference. Also, by applying different decimation numbers, we could have different Gold sequences with the same cross correlation property from the same polynomial.

Table C.1: Meanings of Letters for Primitive Polynomials

Letters	Meanings
A, B, C, D	Not Prime
E, F, G, H	Primitive Prime
A, B, E, F	The roots are linear dependent
C, D, G, H	The roots are linear independent
A,C,E,G	The roots of the reciprocal polynomial are linearly dependent
B,D,F,H	The roots of the reciprocal polynomial are linearly independent

DEGREE 2 01 7H
 DEGREE 3 01 13F
 DEGREE 4 01 23F 03 37D 05 07
 DEGREE 5 01 45E 03 75G 05 67H
 DEGREE 6 01 103F 03 127B 05 147H 07 111A 09 015
 11 155E 21 007
 DEGREE 7 01 211E 03 217E 05 235E 07 367H 09 277E
 11 325G 13 203F 19 313H 21 345G
 DEGREE 8 01 435E 03 567B 05 763D 07 551E 09 675C
 11 747H 13 453F 15 727D 17 023 19 545E
 21 613D 23 543F 25 433B 27 477B 37 537F
 43 703H 45 471A 51 037 85 007
 DEGREE 9 01 1021E 03 1131E 05 1461G 07 1231A 09 1423G
 11 1055E 13 1167F 15 1541E 17 1333F 19 1605G 21 1027A
 23 1751E 25 1743H 27 1617H 29 1553H 35 1401C 37 1157F
 39 1715E 41 1563H 43 1713H 45 1175E 51 1725G 53 1225E
 55 1275E 73 0013 75 1773G 77 1511C 83 1425G 85 1267E

Vita

Candidate's full name: Zhuo Li

University attended: Queen Mary College, University of London, B.Sc.E., 2009

Beijing University of Posts and Telecommunications, B.Sc.E., 2009